

dc step response of induced-charge electro-osmosis between parallel electrodes at large voltages

Hideyuki Sugioka*

Frontier Research Center, Canon Inc., 30-2, Shimomaruko 3-chome, Ohta-ku, Tokyo 146-8501, Japan

(Received 31 October 2013; published 14 July 2014)

Induced-charge electro-osmosis (ICEO) is important since it can be used for realizing high performance microfluidic devices. Here, we analyze the simplest problem of ion relaxation around a circular polarizable cylinder between parallel blocking electrodes in a closed cell by using a multiphysics coupled simulation technique. This technique is based on a combination of the finite-element method and finite-volume method for the Poisson-Nernst-Planck (PNP) equations having a flow term and the Stokes equation having an electric stress term. Through this analysis, we successfully demonstrate that on application of dc voltages, quadrupolar ICEO vortex flows grow during the charging time of the cylinder for both unbounded and bounded problems and decay during the charging time of the parallel electrodes only for the bounded problem using blocking electrodes. Further, by proposing a simple model that considers the two-dimensional (2D) PNP equations analytically, we successfully explain the step response time of the ICEO flow for the both unbounded and bounded problems. Furthermore, at low applied voltages, we find analytical formulations on steady diffused-ion problems and steady ICEO-flow problems and examine that our numerical results agree well with the analytical results. Moreover, by considering an ion-conserving condition with 2D Poisson-Boltzmann equations, we explain significant decrease of the maximum slip velocity at large applied voltages fairly well. We believe that our analysis will contribute greatly to the realistic designs of prospective high-performance microfluidic devices.

DOI: [10.1103/PhysRevE.90.013007](https://doi.org/10.1103/PhysRevE.90.013007)

PACS number(s): 47.57.-s, 85.90.+h, 82.45.-h, 83.50.Lh

I. INTRODUCTION

When an electric field is applied to a polarizable post in an electrolyte, the post is polarized and the electric field near the post initially becomes perpendicular to the surface; then, due to the movement of ions along to the electric field, an electrical double layer is formed; and, finally, the electric field near the post becomes parallel to the surface, and an electro-osmotic flow is generated because of the interaction between the parallel electric field and the charges in the double layer. This phenomena was first predicted by Gamayunov *et al.* [1] in the context of colloids science and later rediscovered and termed as induced charge electro-osmosis (ICEO) by Bazant and Squires [2] in the context of microfluidics. ICEO [2,3] that includes the concept of ac electro-osmosis (ACEO) [4] is important since it can be used for realizing high performance microfluidic devices, such as pumps [5–7], mixers [8–10], valves [11], etc., because of its large flow velocities that are proportional to the square of the applied electric field.

So far, flow velocities on ICEO have been predicted based on the thin-double-layer approximation [12,13] and the predicted large flow velocities in the order of 1 mm/s have been successfully examined in various experiments [5,14]. However, many crucial aspects remain unexplained from the beginning; e.g., Gamayunov *et al.* [1] reported that the vortex flow around metal was sometimes in the opposite direction to that of the theory, although the flow reversal was conjectured to be due to Faradaic reactions [1,3]. Further, the experimental intensities under various experimental conditions are often smaller or much smaller than the predicted values, although the small flow velocity is often explained by the steric effect due to an ion crowding phenomena caused by the application of large voltages [3,15,16]. In addition, as a

serious problem of ICEO applications, the ICEO flow velocity becomes smaller as an initial ion concentration becomes larger, and it becomes zero at about 10 to 100 mM; however, the phenomenon is not explained by the classical theory, although it is also attributed to the steric effect due to an ion crowding phenomena [3,15,16]. Thus, ICEO theory has not been completed yet.

In particular, as was first pointed out by Gamayunov *et al.* [1], the classical theory using the thin-double-layer approximation is basically an approximation that neglects the flow of ions; i.e., flow effects on ion distributions are never considered, although ICEO flow velocities are calculated from a ζ potential and a tangential electric field around a cylinder by neglecting the existence of flows. Thus, strictly speaking, there is possibility that the classical theory is correct only for a small applied voltage (V_0) by which the flow velocities of ions are considered to be zero. Nevertheless, diffused ion dynamics coupled with the generation of ICEO flow at large applied voltages has not been explored enough even numerically by using complete two-dimensional (2D) equations (i.e., 2D Poisson-Nernst-Planck-Stokes equations), although 2D diffused ion dynamics neglecting ICEO flow was explored numerically by Chu and Bazant [17]. Moreover, to the best of our knowledge, complete analytical formulations of 2D ion distributions and ICEO flow distributions in an electrical double layer have not been known yet to the level of analytical formulations that can be compared with the corresponding numerical results even for unbounded problems at small applied voltages, although by using a matched asymptotic approximation Chu and Bazant obtained an approximate charge distribution at small voltages around a conductive sphere [17].

Therefore, in this study, we focus on analyzing the time evolution phenomena of ICEO flow coupled with diffused ion dynamics, on application of large voltages. In particular, we analyze the simplest problem of ion relaxation around a circular polarizable cylinder between parallel blocking

*sugioka.hideyuki@canon.co.jp

electrodes in a closed cell by using a multiphysics coupled simulation technique based on the finite-element method (FEM) and finite-volume method (FVM); specifically, we solve the Stokes equation that includes an electric stress term and the Poisson equation by the FEM and solve the Nernst-Planck (NP) equation that includes a flow term by FVM. Further, we explain a response time of the ICEO flow at large and small applied voltages by proposing a simple model that considers the 2D Poisson-Nernst-Planck (PNP) equations with suitable boundary conditions. Furthermore, we examine the validity of our numerical simulations and clarify the 2D ion and flow distributions in an electrical double layer by obtaining the analytical solutions for the 2D PNP and Stokes equations at small applied voltages. Moreover, we propose a 2D ion-conserving Poisson-Boltzmann theory to explain the significant decrease of the maximum flow velocity at large voltages. It should be noted that this paper does not treat nonblocking electrodes that cause oxidation-reduction reactions and Faraday current, although we use a kind of periodic boundary condition for the ion transportation as a numerical calculation technique in the finite calculation region to consider an unbounded problem.

This paper is presented in nine sections. We begin with five theoretical sections; i.e., in Secs. II, III, IV, V, and VI, we describe (1) a multiphysics calculation technique, (2) a 2D diffused ion theory at small voltages, (3) a 2D ICEO flow theory at small voltages, (4) a 2D large voltage theory on ICEO using an ion-conserving condition, and (5) a simple dc step

response theory based on the 2D PNP equations, respectively. Based on these theories, the time evolution of dc step responses and results of steady state are presented for both unbounded and bounded systems at small and large applied voltages in Sec. VII. Following a discussion in Sec. VIII, our conclusions are summarized in Sec. IX.

II. THEORY (1): NUMERICAL METHOD BASED ON MULTIPHYSICS CALCULATION TECHNIQUE (FE-FV METHOD)

A. Geometry model

Figure 1 shows a schematic of our model used for our 2D time-dependent ICEO analysis of ions in an electrolyte (e.g., water or KCl solution); i.e., as shown in Fig. 1(a), we consider a response of ions and ICEO flows to a dc step voltage in the cell that has an ideally polarizable circular cylinder at the center in an electrolyte between two parallel blocking electrodes. Namely, on application of the dc step voltages, the ions move to the surface of the cylinder, form an electrical double layer, and the ions around the cylinder start moving along the surface, as shown in Fig. 1(a). Here, the dimensional voltage applied to the electrodes is V_0 , the dimensional distance between electrodes is W_0 (e.g., $100 \mu\text{m}$), the dimensional average electric field is $E = V_0/W_0$, the dimensional width of the electrode is $L_0 (=1.5W_0)$, and the dimensional radius of the cylinder is $c_d (=0.1W_0)$; further, $L_1 = L_3 = 0.45W_0$ and $L_2 = 0.6W_0$. It should be noted that we assume that walls

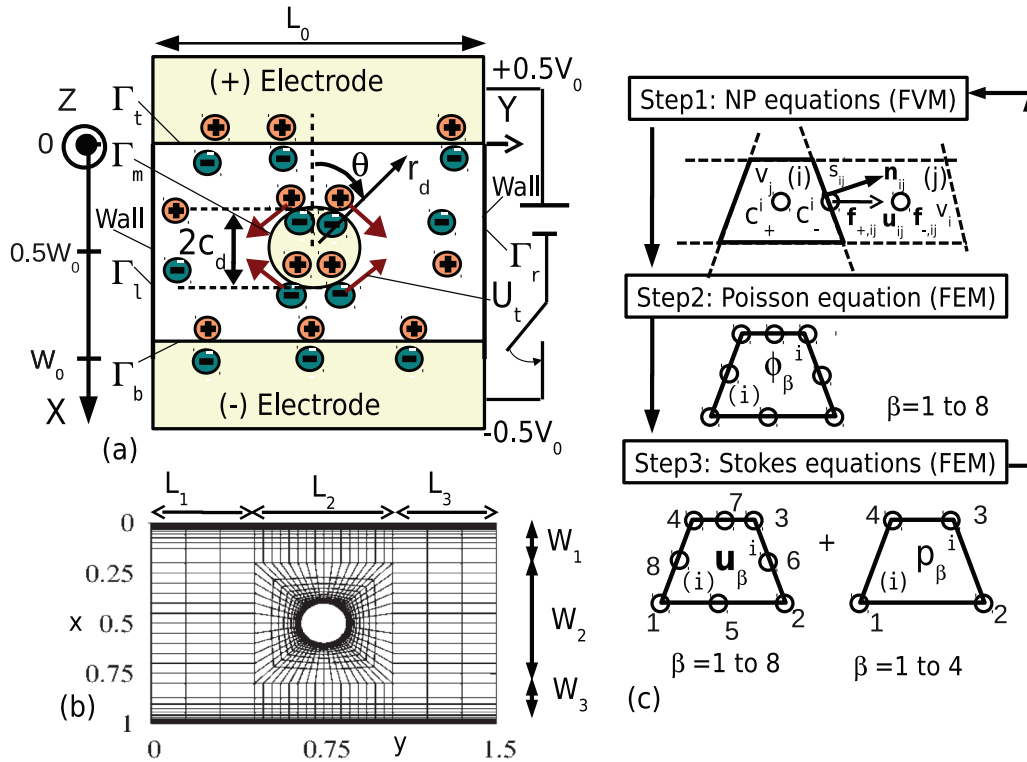


FIG. 1. (Color online) Schematic of our 2D time-dependent ICEO analysis of ions in an electrolyte (e.g., water or KCl solution). (a) ICEO geometry; here, V_0 is the dc voltage suddenly applied to the electrodes, W_0 (e.g., $100 \mu\text{m}$) is the distance between the electrodes, $L_0 (=1.5W_0)$ is the width of the electrode, and $c_d (=0.1W_0)$ is the radius of the circular cylinder of the metal (e.g., Au). (b) Example of an inhomogeneous mesh for numerical calculations; here, $L_1 = L_3 = 0.45W_0$, $L_2 = 0.6W_0$, $W_1 = W_3 = 0.2W_0$, and $W_2 = 0.6W_0$. (c) Multiphysics coupled calculation method using the finite-volume method (FVM) and finite-element method (FEM) for the Stokes-Poisson-Nernst equations.

exist at the left and right sides of the cell and thus the number of ions are conserved in the cell; i.e., we assume a closed system as the first step.

Specifically, Fig. 1(a) corresponds to a bounded problem; thus, the electrical double layers are also formed at the surface of the electrodes. However, for an unbounded problem, we assume a kind of periodic boundary condition at the top and bottom edges of the cell as a numerical calculation technique to calculate the unbounded problem in the finite region. In this case, an electrical double layer does not appear at the top and bottom edges. It should be noted that the analysis for the unbounded problem is needed to examine our numerical calculations and to clarify the intrinsic characteristics on ICEO time response problems.

B. Dimensional basic equations for the diffused ion dynamics coupled with flow

We consider the following initial-boundary-value problem for the 2D PNP equations coupled with the 2D modified (Navier) Stokes equations that include an electrical stress term at $0 \leq X \leq W_0$, $0 \leq Y \leq 1.5W_0$, and $t \geq 0$:

$$\varepsilon \nabla^2 \Phi + \rho_e = 0, \quad (1)$$

$$\frac{\partial C_{\pm}}{\partial t} + \nabla \cdot \mathbf{F}_{\pm} = 0, \quad (2)$$

$$\mathbf{F}_{\pm} = -D \left(\nabla C_{\pm} \pm \frac{ze}{kT} C_{\pm} \nabla \Phi \right) + C_{\pm} \mathbf{u}_d, \quad (3)$$

$$\rho_m \left[\frac{\partial \mathbf{u}_d}{\partial t} + (\mathbf{u}_d \cdot \nabla_n) \mathbf{u}_d \right] = -\nabla P + \mu \nabla^2 \mathbf{u}_d - \rho_e \nabla \Phi, \quad (4)$$

$$\nabla \cdot \mathbf{u}_d = 0,$$

$$\Phi = +0.5V_0 \text{ on } \Gamma_l, \Phi = -0.5V_0 \text{ on } \Gamma_b, \Phi = 0 \text{ on } \Gamma_m, \quad (5)$$

$$\frac{\partial \Phi}{\partial n} = 0 \text{ on } \Gamma_l \text{ and } \Gamma_r, \quad (6)$$

$$\mathbf{F}_{\pm} = 0, \mathbf{u}_d = 0 \text{ on } \Gamma_l, \Gamma_r, \text{ and } \Gamma_m, \quad (7)$$

$$\mathbf{F}_{\pm} = 0, \quad \mathbf{u}_d = 0 \text{ on } \Gamma_l \text{ and } \Gamma_b \text{ (for bounded problems),} \quad (8)$$

$$\mathbf{F}_{\pm} \neq 0, \quad \mathbf{u}_d = 0 \text{ on } \Gamma_l \text{ and } \Gamma_b \text{ (for unbounded problems),} \quad (9)$$

where ε ($\sim 80\varepsilon_0$) is the dielectric permittivity of the solvent (typically water), ε_0 is the vacuum permittivity, Φ is the dimensional potential, $\rho_e (= C_+ - C_-)$ is the dimensional charge, C_+ (C_-) is the dimensional concentration of positive (negative) ions, t is dimensional time, F_+ (F_-) is the dimensional flux of a positive (negative) ion, \mathbf{u}_d is the dimensional flow velocity, ρ_m is the mass density (typically, 1000 kg/m^3), and P is the dimensional pressure. Further, μ (typically, $\sim 1 \text{ mPa s}$) is the viscosity, D ($\sim 10^{-9} \text{ m}^2/\text{s}$) is the ion diffusivity, k is the Boltzmann constant, T is the temperature, and ze is the ion charge. Furthermore, in Eqs. (5)–(9), Γ_l , Γ_r , Γ_t , Γ_b , and Γ_m represent the boundaries of the left side wall, right side wall, top electrode, bottom electrode, and metal post surface,

respectively, as shown in Fig. 1(a). It should be noted that the representative slip velocity on ICEO [2] is

$$U_0^{\text{dimensional}} = \frac{\varepsilon c_d E^2}{\mu}, \quad (10)$$

although the maximum slip velocity around a circular cylinder is usually considered to be $2U_0^{\text{dimensional}}$.

In addition, as mentioned before, we use a kind of periodic boundary conditions for ion transportation for the unbounded problem concerning Eq. (9); i.e., in the multiphysics coupled simulation method (the FE-FV method) described in Appendix A, we assume an artificial flux to expel the ions near the electrode as

$$\mathbf{F}_{\pm}^{X=0, W_0} = -D \frac{C_{\pm}^{X=\Delta X_m/2} - C_{\pm}^{X=W_0-\Delta X_m/2}}{2\Delta X_m} \mathbf{i},$$

where \mathbf{i} is a unit vector in the direction of X , ΔX_m is a X width of the top and bottom cells next to the top and bottom electrodes, respectively, $C_{\pm}^{X=\Delta X_m/2}$ and $C_{\pm}^{X=W_0-\Delta X_m/2}$ are the representative ion concentrations of top and bottom cells, respectively. It should be noted that the artificial flux works stably because it assumes natural diffusion process between the top and bottom surface regions through an external circuit to represent the unbounded condition in the finite calculation region; i.e., through this artificial diffusion process, the increased positive ion at the bottom cell is promptly transported to the top cell, while the increased negative ion at the top cell is promptly transported to the bottom cell; thus, the numbers of ions are safely preserved during calculations. It should be noted that various physical meanings of the ion passing condition at the electrodes are discussed in Appendix C because of the readability. Further, $\mathbf{u}_d = 0$ on the boundaries means $\partial P / \partial n = 0$ and it is naturally considered without inconsistency as a natural boundary condition of the finite-element method described in Appendix C.

C. Dimensionless formulations

For the convenience of the analysis, we use dimensionless formulations corresponding to Eqs. (1)–(9) at $0 \leq x \leq 1$, $0 \leq y \leq 1.5$, and $\tau \geq 0$ as follows:

$$2\varepsilon^2 \nabla_n^2 \phi + \rho = 0, \quad (11)$$

$$\frac{\partial c_{\pm}}{\partial \tau} + \nabla_n \cdot \mathbf{f}_{\pm} = 0, \quad (12)$$

$$\mathbf{f}_{\pm} = -(\nabla_n c_{\pm} \pm c_{\pm} \nabla_n \phi) + c_{\pm} \mathbf{u}, \quad (13)$$

$$\text{Re} \left[\frac{\partial \mathbf{u}}{\partial \tau} + (\mathbf{u} \cdot \nabla_n) \mathbf{u} \right] = -\nabla_n p + \nabla_n^2 \mathbf{u} - F_0 \rho \nabla_n \phi, \quad (14)$$

$$\nabla_n \cdot \mathbf{u} = 0,$$

$$\phi = +0.5v_0 \text{ on } \Gamma_l, \quad \Phi = -0.5v_0 \text{ on } \Gamma_b, \quad \Phi = 0 \text{ on } \Gamma_m, \quad (15)$$

$$\frac{\partial \phi}{\partial n} = 0 \text{ on } \Gamma_l \text{ and } \Gamma_r, \quad (16)$$

$$\mathbf{f}_{\pm} = 0, \quad \mathbf{u} = 0 \text{ on } \Gamma_l, \Gamma_r, \text{ and } \Gamma_m, \quad (17)$$

$$\mathbf{f}_\pm = 0, \quad \mathbf{u} = 0 \text{ on } \Gamma_t \text{ and } \Gamma_b \text{ (for bounded problems),} \quad (18)$$

$$\mathbf{f}_\pm \neq 0, \quad \mathbf{u} = 0 \text{ on } \Gamma_t \text{ and } \Gamma_b \text{ (for unbounded problems),} \quad (19)$$

where $v_0(= V_0/\Phi_c)$, $\phi(= \Phi/\Phi_c)$, $c_\pm(= C_\pm/C_0)$, $\rho(= \rho_e/\rho_{e,c} = c_+ - c_-)$, $\tau(= t/T_0)$, \mathbf{f}_+ (\mathbf{f}_-), $\mathbf{u}(= \mathbf{u}_d/U_c)$, $p(= P/P_c)$, and $(x, y)[= (X/W_0, Y/W_0)]$ are the nondimensional values of an applied voltage, potential, concentration, charge density, time, flux of a positive (negative) ion, flow velocity, pressure, and position, respectively. Here $\epsilon = 1/\kappa = \lambda_D/W_0$, $\lambda_D(= \sqrt{\epsilon kT/2z^2 e^2 C_0})$ denotes the Debye length, $\text{Re} = \rho_m W_0 U_c/\mu = \rho_m D/\mu$ is Reynolds number, $U_c = W_0/T_0 = D/W_0$ is a representative velocity, $T_0 = [W_0^2/D]$ is a diffusion time, and $T_c = [W_0 \lambda_D/D = \epsilon T_0]$ is a (formal) charging time of the system; further, $F_0 = kTC_0 T_0/\mu$, $P_c = \mu/T_0$, $\rho_{e,c} = zeC_0$, and $\Phi_c = kT/ze$; e.g., typically, we obtain $\lambda_D = 1 \mu\text{m}$, $\text{Re} = 10^{-3}$, $T_0 = 10 \text{ s}$, $T_c = 0.1 \text{ s}$, $p_c = 10^{-4} \text{ Pa}$, $\Phi_c = 25.85 \text{ mV}$, and $F_0 = 2494.34$ when $W_0 = 100 \mu\text{m}$, $D = 10^9 \text{ m}^2/\text{s}$, $\mu = 1 \text{ mPa}$, $T = 300 \text{ K}$, and $C_0 = 10^{-7} \text{ M}$. It should be noted that we initially consider the modified incompressible Navier-Stokes (NS) equations [Eq. (14)]; however, because of $\text{Re} \ll 1$, we can neglect the inertial term; thus, we use the modified Stokes equations as follows:

$$-\nabla_n p + \nabla_n^2 \mathbf{u} - F_0 \rho \nabla_n \phi = 0, \quad \nabla_n \cdot \mathbf{u} = 0. \quad (20)$$

Further, the nondimensional typical slip velocity on ICEO corresponding to $U_0^{\text{dimensional}}$ is

$$u_0 \equiv \frac{U_0^{\text{dimensional}}}{U_c} = 2F_0 E_0^2 c \epsilon^2. \quad (21)$$

Furthermore, for the unbounded problem concerning Eq. (19), we assume the artificial flux

$$\mathbf{f}_\pm^{x=0,1} = -\frac{c_\pm^{x=0.5(\Delta X_m/W_0)} - c_\pm^{x=1-0.5(\Delta X_m/W_0)}}{2(\Delta X_m/W_0)} \mathbf{i}$$

at the top and bottom edges.

D. Multiphysics coupled simulation method for the PNP-Stokes equations

To analyze the ion dynamics and ICEO flows numerically, we develop a multiphysics coupled simulation method for the 2D PNP-Stokes equations based on the FVM and the FEM [18,19]. Namely, we first generate unstructured meshes around the metal cylinder and structured meshes in the far positions from the cylinder as shown in Fig. 1(b) and then we solve the NP equation, Poisson equation, and Stokes equations iteratively, as shown in Fig. 1(c). In other words, by solving Eqs. (11)–(20) we calculate the time evolution of c_\pm , ρ , ϕ , p , and \mathbf{u} in the presence of a dc applied voltage v_0 . It should be noted that we use the FEM for the Stokes and Poisson equations [Eqs. (20) and (11)] and the FVM for the NP equations [Eqs. (12) and (13)] because the FEM is convenient for obtaining a suitable second-degree interpolated solution and the FVM is convenient for preserving the number of particles precisely.

Further, to ensure numerical stability of a solver for the Stokes equation, we use a quadrilateral element with eight

nodes and four nodes for \mathbf{u} and p , respectively, while we use a quadrilateral element with eight nodes for ϕ to obtain second-order precision of a solver for the Poisson equations, as shown in Fig. 1(c). Although we just use a fundamental numerical technique for the FEM and FVM [18,19], there are several points we should care to design the coupled simulation tool for the fundamental analysis of the PNP-Stokes equations; thus, we describe the coupled simulation method of the PNP-Stokes equations in Appendix A. Of course, the numerical convergence is verified through multiple runs of different time and space resolutions, and, as mentioned later, we examine that the numerical results at $t = \infty$ agree well with the analytical results predicted by the exact steady PNP solutions at small voltages.

III. THEORY (2): 2D DIFFUSED ION THEORY ON ICEO FOR AN UNBOUNDED PROBLEM AT SMALL VOLTAGES

A. Separation of the Poisson equation for a potential problem at small voltages

At the best of our knowledge, concerning ICEO flows, there is no complete theory that describes inside of the inhomogeneous double layer. It means that so far it has been difficult to show the validity of the numerical calculations completely by the comparison between numerical results and theoretical results. Thus, we derive detail analytical formulations that describes inside and outside of the double layer and examine the numerical results obtained from the FE-FV method described in Sec. II; however, since it is highly complicated, we limit our problem within an unbounded problem as the first step.

Now we restart from Eq. (11) (i.e., the Poisson equation). Since Eq. (11) is a linear equation for ϕ , we can use the principle of superposition; i.e., by assuming that

$$\phi \equiv \phi_{\text{eq}} + \phi_f, \quad (22)$$

we can rewrite Eq. (11) as follows:

$$-2\epsilon^2 \nabla_n^2 (\phi_{\text{eq}} + \phi_f) = \rho. \quad (23)$$

Therefore, we can separate Eq. (23) into two kinds of equations as follows:

$$-2\epsilon^2 \nabla_n^2 \phi_f = 0, \quad (24)$$

$$-2\epsilon^2 \nabla_n^2 \phi_{\text{eq}} = \rho, \quad (25)$$

with the boundary condition that

$$\begin{aligned} \phi_f + \phi_{\text{eq}} &= 0 \quad (\text{at } r = c), \\ \phi_f &\rightarrow E_0 r \cos \theta, \end{aligned} \quad (26)$$

$$\phi_{\text{eq}} \rightarrow 0 \quad (\text{at } r \rightarrow \infty),$$

$$\frac{\partial \phi_f}{\partial r} \rightarrow E_0 \cos \theta, \quad \frac{\partial \phi_{\text{eq}}}{\partial r} \rightarrow 0 \quad (\text{at } r \rightarrow \infty), \quad (27)$$

where the equilibrium potential ϕ_{eq} is the source of ρ and from the definition it approaches zero asymptotically at the infinity. It should be noted that, conceptually, Eqs. (24) and (25) correspond to outside and inside problems, respectively, although they are defined in all concerned regions. In other words, by assuming that the total potential ϕ consists of the

equilibrium potential ϕ_{eq} and the external potential ϕ_f , we separate the problem into the two problems.

B. External (outside) potential at small voltages

Final state: By using cylindrical coordinate (r, θ) , we can rewrite Eq. (24) and related boundary conditions as

$$\frac{\partial^2 \phi_f}{\partial r^2} + \frac{1}{r} \frac{\partial \phi_f}{\partial r} + \frac{1}{r^2} \frac{\partial^2 \phi_f}{\partial \theta^2} = 0. \quad (28)$$

$$\frac{\partial \phi_f}{\partial r} = 0 \quad (\text{at } r = c), \quad (29)$$

$$\phi_f \rightarrow E_0 r \cos \theta \quad (\text{at } r \rightarrow \infty), \quad (30)$$

where $E_0 (\equiv v_0)$ is a nondimensional electric field at $r = \infty$. From Eq. (30), we can assume

$$\phi_f = \tilde{\phi}_f(r) \cos \theta. \quad (31)$$

By instituting Eq. (31) into Eq. (28), we obtain

$$\frac{\partial^2 \tilde{\phi}_f}{\partial r^2} + \frac{1}{r} \frac{\partial \tilde{\phi}_f}{\partial r} - \frac{1}{r^2} \tilde{\phi}_f = 0. \quad (32)$$

This equation is known as the Euler equation, and by transforming it with $r = e^z$ or $z = \ln r$ we obtain the general solution as

$$\tilde{\phi}_f = C'_1 r + C'_2 r^{-1}, \quad (33)$$

where C'_1 and C'_2 are the parameters that are determined from the boundary conditions Eqs. (29) and (30); i.e., $C'_1 = E_0$ and $C'_2 = c^2 E_0$. Therefore, we obtain the solution of Eq. (28) as

$$\phi_f = \left(1 + \frac{c^2}{r^2}\right) E_0 r \cos \theta. \quad (34)$$

Thus, we obtain

$$E_r^f = -\left(1 - \frac{c^2}{r^2}\right) E_0 \cos \theta, \quad (35)$$

$$E_\theta^f = \left(1 + \frac{c^2}{r^2}\right) E_0 \sin \theta. \quad (36)$$

Initial state: It is useful to derive an initial potential ϕ_i . The equation and related boundary conditions are written as

$$\frac{\partial^2 \phi_i}{\partial r^2} + \frac{1}{r} \frac{\partial \phi_i}{\partial r} + \frac{1}{r^2} \frac{\partial^2 \phi_i}{\partial \theta^2} = 0. \quad (37)$$

$$\phi_i = 0 \quad (\text{at } r = c), \quad (38)$$

$$\phi_i \rightarrow E_0 r \cos \theta \quad (\text{at } r \rightarrow \infty). \quad (39)$$

Since Eq. (37) is also transformed into the Euler equation, we obtain

$$\phi_i = \left(1 - \frac{c^2}{r^2}\right) E_0 r \cos \theta. \quad (40)$$

Thus, we obtain

$$E_r^i = -\left(1 + \frac{c^2}{r^2}\right) E_0 \cos \theta, \quad (41)$$

$$E_\theta^i = \left(1 - \frac{c^2}{r^2}\right) E_0 \sin \theta. \quad (42)$$

C. Equilibrium (inside) potential at small voltages

For the steady problem, Nernst-Planck equations [Eqs. (11) and (12)] are simplified into

$$\nabla_n \cdot (\nabla_n c_\pm \pm c_\pm \nabla_n \phi - c_\pm \mathbf{u}) = 0. \quad (43)$$

As explained in Appendix D in detail, from the physical reason that for the appropriate solutions $\nabla_n c_\pm \simeq 0$ in the outside region of the electrical double layer and $\nabla_n \phi_{\text{eq}} \cdot (\nabla_n \phi_f \mp \mathbf{u}) \simeq 0$ in the inside region of the electrical double layer, we obtain that

$$\nabla_n \cdot [\nabla_n c_\pm \pm c_\pm \nabla_n \phi_{\text{eq}}] \simeq 0. \quad (44)$$

Further, since $\nabla_n c_\pm = \nabla_n [c_q e^{\mp \phi_{\text{eq}}}] = \left[\frac{\partial}{\partial \phi_{\text{eq}}} c_q e^{\mp \phi_{\text{eq}}}\right] \nabla_n \phi = \mp c_\pm \nabla_n \phi$, the assumption that

$$c_\pm = c_q e^{\mp \phi_{\text{eq}}} \quad (45)$$

satisfies Eq. (44) and thus satisfies Eq. (43), where c_q is a general nondimensional bulk concentration and it should be determined from the ion-conserving condition [20,21]. Conversely, if we assume Eq. (45), we obtain the physically appropriate solutions that satisfy $\nabla_n c_\pm \simeq 0$ in the outside region of the electrical double layer and $\nabla_n \phi_{\text{eq}} \cdot (\nabla_n \phi_f \mp \mathbf{u}) \simeq 0$ in the inside region of the electrical double layer, as explained later. Thus, we can replace Eq. (43) with Eq. (45) under the ion-conserving condition, as explained in Appendix D in detail.

Therefore, we can write

$$\rho = c_q e^{-\phi_{\text{eq}}} - c_q e^{+\phi_{\text{eq}}} = -2c_q \sinh \phi_{\text{eq}}. \quad (46)$$

At low applied voltages ($v_0 < 1$) we can assume $\sinh \phi_{\text{eq}} \simeq \phi_{\text{eq}}$ and obviously the bulk ion concentration does not change (i.e., $c_q = 1$); thus, we can assume

$$\rho \simeq -2\phi_{\text{eq}} \quad (\text{at } v_0 < 1) \quad (47)$$

instead of Eq. (46). By substituting Eq. (47) into Eq. (25), we obtain a so-called linearized 2D Poisson-Boltzmann (PB) equation that is equivalent with the 2D PNP equations under the condition that $c_q = 1$ as follows:

$$\nabla_n^2 \phi_{\text{eq}} = \kappa^2 \phi_{\text{eq}}. \quad (48)$$

Thus, by using cylindrical coordinate (r, θ) , we obtain

$$\frac{\partial^2 \phi_{\text{eq}}}{\partial r^2} + \frac{1}{r} \frac{\partial \phi_{\text{eq}}}{\partial r} + \frac{1}{r^2} \frac{\partial^2 \phi_{\text{eq}}}{\partial \theta^2} = \kappa^2 \phi_{\text{eq}}, \quad (49)$$

with the boundary condition that

$$\phi_{\text{eq}} + \phi_f = 0 \quad (\text{at } r = c). \quad (50)$$

Since ϕ_f at $r \rightarrow \infty$ is proportional to $\cos \theta$ as shown in Eq. (30), we can assume that $\phi_{\text{eq}}(r, \theta) = \tilde{\phi}_{\text{eq}}(r) \cos \theta$. Thus, from Eq. (49), we obtain

$$\frac{\partial^2 \tilde{\phi}_{\text{eq}}}{\partial r^2} + \frac{1}{r} \frac{\partial \tilde{\phi}_{\text{eq}}}{\partial r} - \left(\kappa^2 + \frac{1}{r^2}\right) \tilde{\phi}_{\text{eq}} = 0. \quad (51)$$

Since Eq. (51) is a modified Bessel equation, the solution is written as

$$\tilde{\phi}_{\text{eq}} = C_1 K_1(\kappa r), \quad (52)$$

where K_1 is a modified Bessel function of the second kind of the first order and C_1 is a parameter that is determined by the

boundary condition; i.e., from Eqs. (50) and (34) [$\phi_f + \phi_{\text{eq}} = 0$ and $\phi_f = 2E_0c \cos \theta$ at $r = c$], we obtain

$$C_1 = -\frac{2E_0c}{K_1(\kappa c)}. \quad (53)$$

Therefore, we obtain

$$\phi_{\text{eq}} = -\frac{2E_0c}{K_1(\kappa c)} K_1(\kappa r) \cos \theta. \quad (54)$$

Thus, from Eq. (47), we obtain

$$\rho \simeq 2 \left[\frac{2E_0c}{K_1(\kappa c)} \right] K_1(\kappa r) \cos \theta. \quad (55)$$

D. Total potential at small voltages

From Eqs. (34) and (54), we obtain

$$\begin{aligned} \phi &= \phi^f + \phi^{\text{eq}} \\ &= \left(1 + \frac{c^2}{r^2}\right) E_0 r \cos \theta - \left[\frac{2E_0c}{K_1(\kappa c)} \right] K_1(\kappa r) \cos \theta. \end{aligned} \quad (56)$$

Thus, we obtain

$$\begin{aligned} E_\theta &= -\frac{1}{r} \frac{\partial \phi}{\partial \theta} \\ &= \left(1 + \frac{c^2}{r^2}\right) E_0 \sin \theta - \left[\frac{2E_0c}{K_1(\kappa c)} \right] \frac{K_1(\kappa r)}{r} \sin \theta, \end{aligned} \quad (57)$$

$$\begin{aligned} E_r &= -\frac{\partial \phi}{\partial r} \\ &= -\left(1 - \frac{c^2}{r^2}\right) E_0 \cos \theta + \left[\frac{2E_0c}{K_1(\kappa c)} \right] \frac{\partial K_1(\kappa r)}{\partial r} \cos \theta, \end{aligned} \quad (58)$$

where

$$\frac{\partial K_1(\kappa r)}{\partial r} = -\frac{\kappa}{2} [K_0(\kappa r) + K_2(\kappa r)],$$

which is a well-known relation for Bessel functions. Further, from Eqs. (55), (57), and (58), we obtain the electric force term as

$$F_0 \rho E_\theta = F_0 \left[p_1 E_0 \left(1 + \frac{c^2}{r^2}\right) K_1(\kappa r) - p_1^2 \frac{K_1(\kappa r)^2}{r} \right] \sin 2\theta, \quad (59)$$

$$\begin{aligned} F_0 \rho E_r &= F_0 \left[-p_1 E_0 \left(1 - \frac{c^2}{r^2}\right) K_1(\kappa r) \right. \\ &\quad \left. + p_1^2 \frac{\partial K_1(\kappa r)}{\partial r} K_1(\kappa r) \right] 2 \cos^2 \theta. \end{aligned} \quad (60)$$

where $p_1 = \frac{2E_0c}{K_1(\kappa c)}$. Further, for convenience later, we transform $F_0 \rho \mathbf{E}$ for the small voltage problem as follows:

$$\begin{aligned} F_0 \rho \mathbf{E} &= F_0 (-2\phi_{\text{eq}}) [-\nabla(\phi_{\text{eq}} + \phi_f)] \\ &= \nabla(F_0 \phi_{\text{eq}}^2) + 2F_0 \phi_{\text{eq}} \nabla \phi_f. \end{aligned} \quad (61)$$

Thus, since $\text{rot grad} \equiv 0$, we obtain

$$T = \hat{z} \cdot \text{rot}(F_0 \rho \mathbf{E}) = \hat{z} \cdot \text{rot}(2F_0 \phi_{\text{eq}} \nabla \phi_f) = \tilde{T}(r) \sin 2\theta, \quad (62)$$

where

$$\tilde{T}(r) = F_0 p_1 E_0 \left[\left(1 - \frac{c^2}{r^2}\right) \frac{K_1(\kappa r)}{r} - \left(1 + \frac{c^2}{r^2}\right) \frac{\partial K_1(\kappa r)}{\partial r} \right]. \quad (63)$$

IV. THEORY (3): 2D FLOW THEORY ON ICEO FOR AN UNBOUNDED PROBLEM AT SMALL VOLTAGES

A. Separation of the Stokes equation on ICEO at small voltages

Similarly to the above potential problem, since the Stokes equation [Eq. (20)] is also a linear equation for \mathbf{u} , we can use the principle of superposition again; thus, by assuming that

$$\mathbf{u} \equiv \mathbf{u}_{\text{eq}} + \mathbf{u}_f, \quad p = p_f + p_{\text{eq}}, \quad (64)$$

we can rewrite the Stokes equation as follows:

$$\nabla_n^2 (\mathbf{u}_{\text{eq}} + \mathbf{u}_f) = \nabla_n (p_f + p_{\text{eq}}) - F_0 \rho \mathbf{E}, \quad (65)$$

$$\nabla_n \cdot (\mathbf{u}_{\text{eq}} + \mathbf{u}_f) = 0.$$

Thus, we can separate Eq. (65) into the two equations as follows:

$$\nabla_n^2 \mathbf{u}_f = \nabla_n p_f, \quad \nabla_n \cdot \mathbf{u}_f = 0, \quad (66)$$

$$\nabla_n^2 \mathbf{u}_{\text{eq}} = \nabla_n (p_f + p_{\text{eq}}) - F_0 \rho \mathbf{E}, \quad \nabla_n \cdot \mathbf{u}_{\text{eq}} = 0, \quad (67)$$

where the term $\nabla_n p_f$ is a driving force of \mathbf{u}_f and \mathbf{E} is a nondimensional electric field.

B. Outside solution on ICEO at small voltages

By using the fact that $\text{rot} \nabla^2 = \nabla^2 \text{rot}$ and $\text{rot grad} \equiv 0$, we can transform the first equation of Eq. (66) into

$$\nabla_n^2 \text{rot} \mathbf{u}_f = 0, \quad (68)$$

where $\text{rot} \mathbf{u}_f = \frac{1}{r} \left[\frac{\partial}{\partial r} (r u_\theta) - \frac{\partial u_r}{\partial r} \right] \mathbf{k}$. Further, instead of the second equation of Eq. (66), we use

$$u_\theta^f = -\frac{\partial \Phi^{\text{st},f}}{\partial r}, \quad u_r^f = +\frac{1}{r} \frac{\partial \Phi^{\text{st},f}}{\partial \theta}, \quad (69)$$

where $\Phi^{\text{st},f}$ is a Stokes potential and Eq. (69) satisfies the second equation of Eq. (66). Thus, by substituting Eq. (69) into Eq. (68), we obtain

$$\begin{aligned} \nabla_n^4 \Phi^{\text{st},f} &= \nabla_n^2 (\nabla_n \Phi^{\text{st},f}) \\ &= \left[\frac{\partial^2}{\partial r^2} + \frac{1}{r} \frac{\partial}{\partial r} + \frac{1}{r^2} \frac{\partial^2}{\partial \theta^2} \right]^2 \Phi^{\text{st},f} \\ &= 0. \end{aligned} \quad (70)$$

This equation is termed the biharmonic equation and the 2D solution in the cylindrical coordinate is well known. Thus, by selecting the term only related to $\sin 2\theta$, we obtain

$$\Phi^{\text{st},f} = (C_2 r^{-2} + C_3 + C_4 r^2 + C_5 r^4) \sin 2\theta, \quad (71)$$

where C_2, C_3, C_4 , and C_5 are determined from the boundary condition; i.e., since $\Phi^{\text{st},f} = 0$ at $r = \infty$, we obtain $C_4 = C_5 = 0$. Thus, we obtain

$$\Phi^{\text{st},f} = (C_2 r^{-2} + C_3) \sin 2\theta. \quad (72)$$

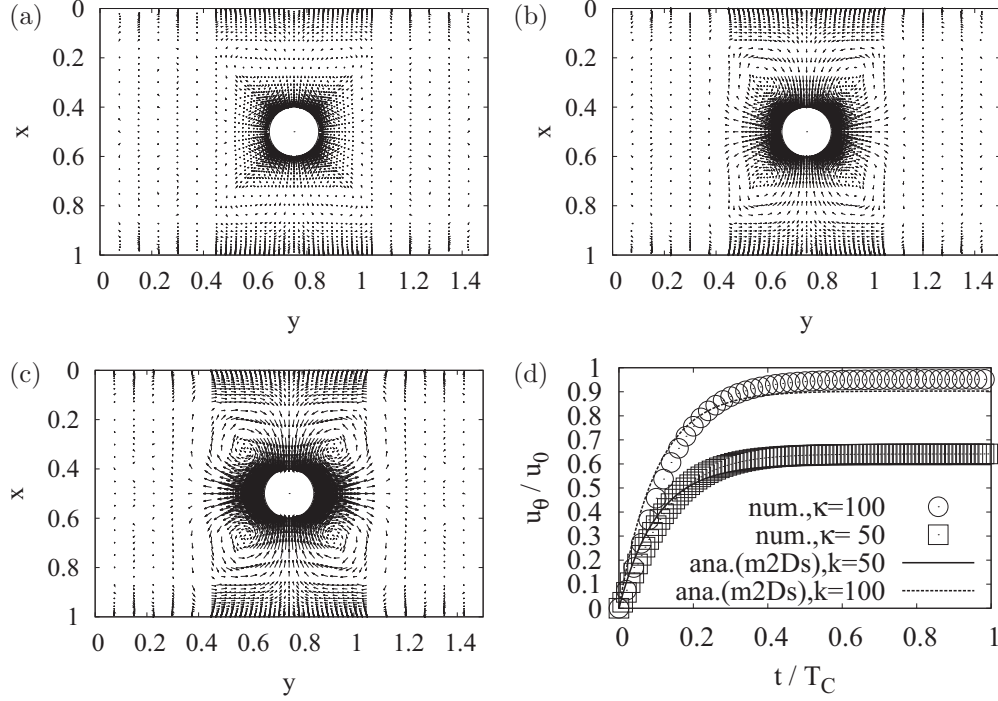


FIG. 2. Time evolution of ICEO flow fields for an unbounded problem at small applied electric field ($E_0 = v_0 = 0.1$). (a), (b), and (c) show the flow fields at $t/T_c = 0.02, 0.10$, and 0.40 , respectively, at $\kappa = 100$ and $c = 0.1$; in (d), the broken and solid lines show the analytical results obtained by Eq. (174) with Eq. (97) at $\kappa = 100$ and 50 , respectively, while the circles and squares show the numerical results by use of the FE-FV method at $\kappa = 100$ and 50 , respectively.

Therefore, by substituting Eq. (72) into Eq. (69), we obtain

$$u_\theta^f = 2C_2 r^{-3} \sin 2\theta, \quad (73)$$

$$u_r^f = 2(C_2 r^{-3} + C_3 r^{-1}) \cos 2\theta. \quad (74)$$

It should be noted that the same kind of outer solutions [Eqs. (73) and (74)] are obtained by Gomayunov *et al.* [1] and Squires and Bazant [13].

C. Pressure problem

Although we need not to consider a pressure value in the concerning formulations, if we need to obtain P_f , we can obtain it from Eq. (66). That is, by using vector equivalence with the continuum equation, we obtain $\nabla_n^2 \mathbf{u}_f \equiv \nabla_n (\nabla_n \cdot \mathbf{u}_f) - \nabla_n \times \nabla_n \times \mathbf{u}_f = -\nabla_n \times \nabla_n \times \mathbf{u}_f$. Therefore, we can transform Eq. (66) into

$$\frac{\partial}{\partial r} \left[\frac{1}{r} \frac{\partial}{\partial r} (r u_\theta^f) - \frac{1}{r} \frac{\partial u_r^f}{\partial \theta} \right] = \frac{1}{r} \frac{\partial p_f}{\partial \theta} \quad (\theta \text{ component}), \quad (75)$$

$$-\frac{1}{r} \frac{\partial}{\partial \theta} \left[\frac{1}{r} \frac{\partial}{\partial r} (r u_\theta^f) - \frac{1}{r} \frac{\partial u_r^f}{\partial \theta} \right] = \frac{\partial p_f}{\partial r} \quad (r \text{ component}). \quad (76)$$

By substituting Eqs. (73) and (74) into Eq. (75), we obtain

$$p_f = C_3 r^{-2} \cos 2\theta. \quad (77)$$

D. Inside solution on ICEO at small voltages

Similarly to the outside problem, by using the fact that $\text{rot} \nabla^2 = \nabla^2 \text{rot}$ and $\text{rot} \text{grad} \equiv 0$, we transform Eq. (67)

into

$$\nabla_n^4 \Phi^{\text{st,eq}} = \hat{z} \cdot \text{rot}(F_0 \rho \mathbf{E}) = T, \quad (78)$$

where \hat{z} is a unit vector in the direction of z (in Fig. 2) and $\Phi^{\text{st,eq}}$ is a Stokes potential that gives velocities as

$$u_\theta^{\text{eq}} = -\frac{\partial \Phi^{\text{st,eq}}}{\partial r}, \quad (79)$$

$$u_r^{\text{eq}} = +\frac{1}{r} \frac{\partial \Phi^{\text{st,eq}}}{\partial \theta}. \quad (80)$$

Since the general solution of the homogeneous equation corresponding to Eq. (78) is the same as that of Eq. (70), we just consider the particular solution of Eq. (78) for $\Phi^{\text{st,eq}}$. Thus, by introducing v , we separate Eq. (78) into

$$\nabla_n^2 \Phi^{\text{st,eq}} = v, \quad (81)$$

$$\nabla_n^2 v = \text{rot}(F_0 \rho \mathbf{E}) \hat{z}, \quad (81)$$

with the boundary condition that

$$\nabla_n \Phi^{\text{st,eq}} = \nabla_n v = \Phi^{\text{st,eq}} = v = 0 \quad (\text{at } r \rightarrow \infty), \quad (83)$$

where

$$\nabla_n^2 = \frac{\partial^2}{\partial r^2} + \frac{1}{r} \frac{\partial}{\partial r} + \frac{1}{r^2} \frac{\partial^2}{\partial \theta^2}. \quad (84)$$

Further, since $T = \hat{z} \cdot \text{rot}(F_0 \rho \mathbf{E}) = \tilde{T}(r) \sin 2\theta$ as shown in Eq. (62), we can assume that

$$\Phi^{\text{st,eq}} = \check{\Phi}^{\text{st,eq}} \sin 2\theta, \quad (85)$$

$$v = \check{v} \sin 2\theta. \quad (86)$$

Thus, we obtain

$$\left[\frac{\partial^2}{\partial r^2} + \frac{1}{r} \frac{\partial}{\partial r} - \frac{4}{r^2} \right] \tilde{\Phi}^{\text{st,eq}} = \tilde{v}, \quad (87)$$

$$\left[\frac{\partial^2}{\partial r^2} + \frac{1}{r} \frac{\partial}{\partial r} - \frac{4}{r^2} \right] \tilde{v} = \tilde{T}. \quad (88)$$

Since Eqs. (87) and (88) are inhomogeneous linear equations of second order, we obtain the analytical formulations of the particular solutions; i.e., by using the two kind solutions ($r^{\pm 2}$) of the corresponding homogeneous equations (Euler equation), we obtain

$$\begin{aligned} \tilde{v}(r) &= +r^2 \int_r^\infty \frac{r'^{-2} \tilde{T}}{D} dr' - r^{-2} \int_r^\infty \frac{r'^2 \tilde{T}}{D} dr' \\ &= -\frac{r^2}{4} \int_r^\infty \frac{\tilde{T}}{r'} dr' + \frac{1}{4r^2} \int_r^\infty r'^3 \tilde{T} dr', \end{aligned} \quad (89)$$

where $D = r^2 \frac{\partial r^{-2}}{\partial r} - r^{-2} \frac{\partial r^2}{\partial r} = -\frac{4}{r}$. Similarly, we obtain

$$\tilde{\Phi}^{\text{st,eq}} = -\frac{r^2}{4} \int_r^\infty \frac{\tilde{v}}{r'} dr' + \frac{1}{4r^2} \int_r^\infty r'^3 \tilde{v} dr'. \quad (90)$$

Thus, by using Eqs. (79) and (80), we obtain

$$u_\theta^{\text{eq}} = \tilde{u}_\theta^{\text{eq}}(r) \sin 2\theta, \quad (91)$$

$$u_r^{\text{eq}} = \tilde{u}_r^{\text{eq}}(r) \cos 2\theta, \quad (92)$$

where

$$\tilde{u}_\theta^{\text{eq}}(r) = \frac{r}{2} \int_r^\infty \frac{\tilde{v}}{r'} dr' + \frac{1}{2r^3} \int_r^\infty r'^3 \tilde{v} dr' - \frac{r^2}{4} \frac{\tilde{v}}{r} + \frac{1}{4r^2} r^3 \tilde{v}, \quad (93)$$

$$\tilde{u}_r^{\text{eq}}(r) = -\frac{r}{2} \int_r^\infty \frac{\tilde{v}}{r'} dr' + \frac{1}{2r^3} \int_r^\infty r'^3 \tilde{v} dr'. \quad (94)$$

E. Total solution on ICEO at low voltages

Since $u_\theta^{\text{eq}}(r) + u_\theta^f(r) = 0$ and $u_r(r)^{\text{eq}} + u_r^f(r) = 0$ at $r = c$, we obtain that

$$C_2 = \frac{c^3}{2} \tilde{u}_\theta^{\text{eq}}(c), \quad (95)$$

$$C_3 = -\frac{c}{2} [\tilde{u}_\theta^{\text{eq}}(c) + \tilde{u}_r^{\text{eq}}(c)]. \quad (96)$$

Thus, from Eqs. (64), (73), (74), (91), and (92), we obtain

$$\begin{aligned} u_\theta^{\text{Model D}} &= \left[\tilde{u}_\theta^{\text{eq}}(r) + \frac{2C_2}{r^3} \right] \sin 2\theta \\ &= \tilde{u}_\theta^{\text{eq}}(c) \left[\frac{\tilde{u}_\theta^{\text{eq}}(r)}{\tilde{u}_\theta^{\text{eq}}(c)} + \frac{c^3}{r^3} \right] \sin 2\theta, \end{aligned} \quad (97)$$

$$\begin{aligned} u_r^{\text{Model D}} &= \left[\tilde{u}_r^{\text{eq}}(r) + \frac{2C_2}{r^3} + \frac{2C_3}{r} \right] \cos 2\theta \\ &= \left[\tilde{u}_r^{\text{eq}}(r) + \frac{c^3}{r^3} \tilde{u}_\theta^{\text{eq}}(r) - \frac{c}{r} \tilde{u}_r^{\text{eq}}(c) - \frac{c}{r} \tilde{u}_\theta^{\text{eq}}(c) \right] \cos 2\theta. \end{aligned} \quad (98)$$

It should be noted that Eqs. (93) and (94) can be calculated numerically since they just include definite integrals. Further, we call this method ‘‘Model D’’ and various approximations are presented in Appendix B as Models A to C.

V. THEORY (4): LARGE VOLTAGE THEORY ON ICEO USING AN ION-CONSERVING CONDITION

A. 2D nonlinear Poisson-Boltzmann equation

By substituting Eq. (46) into Eq. (25), we obtain the 2D nonlinear Poisson-Boltzmann (PB) equation as follows:

$$\nabla_n^2 \phi_{\text{eq}} = \kappa_q^2 \sinh \phi_{\text{eq}}, \quad (99)$$

where $\kappa_q = \kappa \sqrt{c_q}$. By multiplying Eq. (99) by $\nabla_n \phi_{\text{eq}}$, we obtain

$$\nabla_n \phi_{\text{eq}} \nabla_n^2 \phi_{\text{eq}} = (\nabla_n \phi_{\text{eq}}) \kappa_q^2 \sinh \phi_{\text{eq}}. \quad (100)$$

By using the relation that $\nabla_n \phi_{\text{eq}} \nabla_n^2 \phi_{\text{eq}} = \nabla_n (\frac{1}{2} (\nabla_n \phi_{\text{eq}})^2)$ and $(\nabla_n \phi_{\text{eq}}) \kappa_q^2 \sinh \phi_{\text{eq}} = \nabla_n (\kappa_q^2 \cosh \phi_{\text{eq}})$, we obtain

$$\nabla_n (\frac{1}{2} (\nabla_n \phi_{\text{eq}})^2) = \nabla_n (\kappa_q^2 \cosh \phi_{\text{eq}}). \quad (101)$$

Thus, we obtain

$$(\nabla_n \phi_{\text{eq}})^2 = 2\kappa_q^2 \cosh \phi_{\text{eq}} + C_5, \quad (102)$$

where C_5 is an integral constant. By using the boundary condition that $\nabla_n \phi_{\text{eq}} = 0$ at $r \rightarrow \infty$, we obtain

$$C_5 = -2\kappa_q^2 \cosh \phi_{\text{eq}}. \quad (103)$$

Thus, we obtain

$$|\nabla_n \phi_{\text{eq}}| = \sqrt{2\kappa_q^2 (\cosh \phi_{\text{eq}} - 1)}. \quad (104)$$

B. Solution of 2D nonlinear Poisson-Boltzmann equation

Since $|\nabla_n \phi_{\text{eq}}| = \sqrt{(\frac{\partial \phi_{\text{eq}}}{\partial r})^2 + (\frac{1}{r} \frac{\partial \phi_{\text{eq}}}{\partial \theta})^2}$, we obtain

$$\sqrt{\left(\frac{\partial \phi_{\text{eq}}}{\partial r} \right)^2 + \left(\frac{1}{r} \frac{\partial \phi_{\text{eq}}}{\partial \theta} \right)^2} = \sqrt{2\kappa_q^2 (\cosh \phi_{\text{eq}} - 1)}. \quad (105)$$

Here, since $\epsilon \ll 1$ in our calculations, we can assume that $\frac{\partial}{\partial \theta} = 0$ as the first step. Thus, we can approximate Eq. (105) as follows:

$$\frac{\partial \phi_{\text{eq}}}{\partial r} \simeq -\sqrt{2\kappa_q^2 (\cosh \phi_{\text{eq}} - 1)} = -2\kappa_q \sinh \frac{\phi_{\text{eq}}}{2}. \quad (106)$$

It should be noted that the negative sign is needed since $\phi_{\text{eq}} < 0$, $\sinh \frac{\phi_{\text{eq}}}{2} < 0$, and $\frac{\partial \phi_{\text{eq}}}{\partial r} > 0$ in the range that $r \geq c$ and $x \leq 0$. Since Eq. (106) is the same as the Eq. (A4) in our previous paper on a 1D problem [20], our 2D problem is transformed into the 1D problem.

That is, by setting $y = e^{\frac{\phi_{\text{eq}}}{2}}$, we obtain that $\phi = 2 \ln y$, $\frac{\partial \phi_{\text{eq}}}{\partial r} = \frac{2}{y} \frac{\partial y}{\partial x}$, and $e^{-\frac{\phi_{\text{eq}}}{2}} = \frac{1}{y}$. By using these relations and Eq. (106), we obtain

$$\frac{2}{y} \frac{\partial y}{\partial r} = -2\kappa_q \frac{y - \frac{1}{y}}{2}. \quad (107)$$

Thus, by integrating Eq. (107), we obtain

$$\int \frac{dy}{y^2 - 1} = \int \frac{\kappa_q}{2} dr, \quad (108)$$

$$\frac{1}{2} \ln \frac{y - 1}{y + 1} = -\frac{\kappa_q}{2} r + C_6, \quad (109)$$

$$\frac{e^{\frac{\phi_{\text{eq}}}{2}} - 1}{e^{\frac{\phi_{\text{eq}}}{2}} + 1} = C_7 e^{-\kappa_q r} = B, \quad (110)$$

where C_6 is a constant and $C_7 = e^{C_6}$. Therefore,

$$\phi_{\text{eq}} = 2 \ln \frac{1 + B}{1 - B}. \quad (111)$$

By considering the boundary condition that $\phi_{\text{eq}}(c) = -\phi_f(c) = -2E_0 c \cos \theta$, we obtain

$$\frac{e^{\frac{\phi_{\text{eq}}(c)}{2}} - 1}{e^{\frac{\phi_{\text{eq}}(c)}{2}} + 1} = \tanh \frac{\phi_{\text{eq}}(c)}{4} = C_7 e^{-\kappa_q c}. \quad (112)$$

Thus,

$$C_7 = e^{\kappa_q c} \tanh \frac{\phi_{\text{eq}}(c)}{4}, \quad (113)$$

$$B = e^{-\kappa_q(r-c)} \tanh \frac{\phi_{\text{eq}}(c)}{4}. \quad (114)$$

Therefore, from Eqs. (111) and (114), we obtain

$$\phi_{\text{eq}}(r) = 2 \ln \left[\frac{1 + e^{-\kappa_q(r-c)} \tanh \frac{\phi_{\text{eq}}(c)}{4}}{1 - e^{-\kappa_q(r-c)} \tanh \frac{\phi_{\text{eq}}(c)}{4}} \right], \quad (115)$$

where $\phi_{\text{eq}}(c) = -\phi_f(c) = -2E_0 c \cos \theta$.

C. 2D ion-conserving condition at large voltages

As mentioned before, for the steady problem, the Nernst-Planck equations [Eqs. (11) and (12)] are simplified into

$$\nabla_n \cdot (\nabla_n c_{\pm} \pm c_{\pm} \nabla_n \phi - c_{\pm} \mathbf{u}) = 0, \quad (116)$$

and it shows an ion-conserving condition that consider both in- and out-flows in a closed region. Further, as mentioned before (and explained in Appendix D in detail), Eq. (116) is approximately replaced by

$$c_{\pm} = c_q e^{\mp \phi_{\text{eq}}} \quad (117)$$

with the ion-conserving condition even for large applied voltages. In particular, since here we assume that

$$\frac{\partial \phi_{\text{eq}}}{\partial \theta} \simeq 0, \quad (118)$$

the requirement condition of Eq. (D8) in Appendix D is obviously satisfied in the electrical double layer; i.e.,

$$\nabla_n \phi_{\text{eq}} \cdot (\nabla_n \phi_f \mp \mathbf{u}) = 0; \quad (119)$$

thus, we can safely replace Eq. (116) by Eq. (117) in this case.

However, differing from the small voltage problem in Sec. III, c_q must be determined from the ion-conserving condition for the large voltage problem, similarly to the 1D ion-conserving Poisson-Boltzmann theory [20]; i.e., we require an ion-conserving condition that

$$\begin{aligned} & \int_0^{\frac{\pi}{2}} \int_c^{c+d^{\text{eff}}} (c_q e^{-\phi_{\text{eq}}} + c_q e^{+\phi_{\text{eq}}}) r dr d\theta \\ &= \int_0^{\frac{\pi}{2}} \int_c^{c+d^{\text{eff}}} (c_+^{\text{initial}} + c_-^{\text{initial}}) r dr d\theta, \end{aligned} \quad (120)$$

where the left- and right-side integral values are a nondimensional total ion number for final (steady) and initial states, respectively, and $c_+^{\text{initial}} (= 1)$ [$c_-^{\text{initial}} (= 1)$] is an initial positive (negative) ion concentration. Please note that because of the symmetry of the system and under the assumption that the ion concentrations do not change at $r > c + d^{\text{eff}}$, we just consider the region that $c \leq r \leq c + d^{\text{eff}}$ and $0 \leq \theta \leq \pi/2$, where $d^{\text{eff}} (\geq \epsilon)$ is a distance concerning the ion-conserving condition. It should be noted that, differing from the 1D problem on parallel electrodes in the closed cell [20], the current problem requires the discussion on an ion-conserving condition for the open system concerning d^{eff} . That is, for the steady state we assume that the ion concentration c_{\pm} is constant at $r > c + d^{\text{eff}}$ because of the appearance of the quasiequilibrium state in which the values of inflow and outflow are balanced, although, unfortunately, we have not known the analytical expression yet, as mentioned later. Of course, we tried the assumption that c_q is determined by the similar integration over the whole region (i.e, $0 \leq x \leq 1$ and $0 \leq y \leq 1.5$); however, we easily understand that the treatment just provides unrealistic results compared to our reliable numerical results that are examined at least for the small voltage problem. Further, researchers may consider that ions are moved to the surface from the infinitely far region and formed electrical double layer for the steady state; however, now we believe that in a nonequilibrium system, the stable local quasiequilibrium state (in which the values of inflow and outflow are balanced) appears in the charging time of the circular cylinder.

Mathematically, the 2D condition of Eq. (120) is almost same as the 1D condition of our previous paper [20]; thus, we can simplify the condition similarly. That is, by substituting Eq. (115) into Eq. (120) with the approximation that $r dr d\theta \simeq c dr d\theta$ that is consistent with the assumption of Eq. (115), we obtain

$$\begin{aligned} & c_q \int_0^{\frac{\pi}{2}} \int_0^{d^{\text{eff}}} \left[\left(\frac{1 + \alpha e^{-x\kappa_q}}{1 - \alpha e^{-x\kappa_q}} \right)^2 + \left(\frac{1 - \alpha e^{-x\kappa_q}}{1 + \alpha e^{-x\kappa_q}} \right)^2 \right] dx d\theta \\ &= 2d^{\text{eff}} \frac{\pi}{2}, \end{aligned} \quad (121)$$

where $\alpha = \tanh(-\phi_f(c)/4)$ and $x = r - c$. By using $t = \alpha e^{-x\kappa_q}$ and $dx = -dt/\kappa_q t$, we obtain

$$\frac{-c_q}{\kappa_q} \int_0^{\frac{\pi}{2}} \int_{\alpha}^{\alpha e^{-\kappa_q d^{\text{eff}}}} \left[\left(\frac{1+t}{1-t} \right)^2 \frac{1}{t} + \left(\frac{1-t}{1+t} \right)^2 \frac{1}{t} \right] dx = \pi d^{\text{eff}}. \quad (122)$$

Since $\frac{(1+t)^2}{(1-t)^2} \frac{1}{t} = \frac{4}{(1-t)^2} + \frac{1}{t} \frac{(1-t)^2}{(1+t)^2} = \frac{-4}{(1+t)^2} + \frac{1}{t}$ and $\frac{4}{(1+t)^2} - \frac{4}{(1-t)^2} = \frac{16t}{(t^2-1)^2}$, we obtain $\frac{(1+t)^2}{(1-t)^2} \frac{1}{t} + \frac{(1-t)^2}{(1+t)^2} \frac{1}{t} = \frac{16t}{(t^2-1)^2} + \frac{2}{t}$. Thus,

$$\frac{-c_q}{\kappa_q} \int_0^{\frac{\pi}{2}} \int_{\alpha}^{\alpha e^{-\kappa_q d^{\text{eff}}}} \left[\frac{16t}{(t^2-1)^2} + \frac{2}{t} \right] dx d\theta = \pi d^{\text{eff}}. \quad (123)$$

Since $\int t/(t^2-1)^2 dt = -1/2(x^2-1)$ and $\int 1/t dt = \ln t$, we obtain

$$\frac{c_q}{\kappa_q} \int_0^{\frac{\pi}{2}} \left[\frac{8}{t^2-1} - \ln t \right]_{\alpha}^{\alpha e^{-\kappa_q d^{\text{eff}}}} d\theta = \pi d^{\text{eff}}. \quad (124)$$

Thus, to conserve the number of ions, c_q must satisfy the following equation:

$$c_q \int_0^{\frac{\pi}{2}} \left[\frac{8}{\kappa \sqrt{c_q}} \left(\frac{1}{\alpha^2 e^{-2\kappa_q d^{\text{eff}}} - 1} - \frac{1}{\alpha^2 - 1} \right) + 2d^{\text{eff}} \right] d\theta = \pi d^{\text{eff}}, \quad (125)$$

where we use $\kappa_q = \kappa \sqrt{c_q}$ to clarify the problem. If $\kappa \gg 1$ and $\kappa_q \gg 1$, we can neglect the term $\alpha^2 e^{-2\kappa_q d^{\text{eff}}}$; thus,

$$\frac{1}{\alpha^2 e^{-2\kappa_q d^{\text{eff}}} - 1} - \frac{1}{\alpha^2 - 1} = \frac{\alpha^2 - \alpha^2 e^{-2\kappa_q d^{\text{eff}}}}{(1 - \alpha^2 e^{-2\kappa_q d^{\text{eff}}})(1 - \alpha^2)} \simeq \frac{\alpha^2}{1 - \alpha^2}. \quad (126)$$

Therefore, we can transform Eq. (125) into

$$c_q \int_0^{\frac{\pi}{2}} \left[\frac{8}{\kappa d^{\text{eff}} \sqrt{c_q}} \left(\frac{\alpha^2}{1 - \alpha^2} \right) + 2 \right] d\theta = \pi. \quad (127)$$

Because Eq. (127) is a quadratic equation for $X = \sqrt{c_q}$, we obtain

$$X^2 + 2AX - 1 = 0, \quad (128)$$

where

$$A = \frac{4}{\kappa d^{\text{eff}} \pi} \int_0^{\frac{\pi}{2}} \frac{\alpha^2}{1 - \alpha^2} d\theta = \frac{2}{\kappa d^{\text{eff}} \pi} \int_0^{\frac{\pi}{2}} \sinh^2 \left[-\frac{E_0 c \cos(\theta)}{2} \right] d\theta. \quad (129)$$

Therefore,

$$c_q = (-A + \sqrt{1 + A^2})^2. \quad (130)$$

This is an ion-conserving condition for the 2D problem and only under this condition is the nonlinear Poisson-Boltzmann equation [Eq. (99)] equivalent to the Poisson-Nernst-Planck equations.

D. 2D flow theory at large voltages

For the convenience of the reader, we rewrite Eq. (46),

$$\rho = -2c_q \sinh \phi_{\text{eq}}.$$

Since we derive ϕ_{eq} and c_q in Eqs. (115) and (130), we can calculate ρ at large applied voltages. Further, from Eq. (115)

[or Eq. (111)], we obtain

$$\begin{aligned} E_{\theta}^{\text{eq}} &= -\frac{1}{r} \frac{\partial \phi}{\partial \theta} \\ &= -2 \frac{1-B}{1+B} \frac{(1-B)B_{\theta} + (1+B)B_{\theta}}{(1-B)^2} \frac{1}{r} \\ &= -\frac{4B_{\theta}}{1-B^2} \frac{1}{r}, \end{aligned} \quad (131)$$

$$\begin{aligned} E_r^{\text{eq}} &= -\frac{\partial \phi}{\partial r} \\ &= -2 \frac{1-B}{1+B} \frac{(1-B)B_r + (1+B)B_r}{(1-B)^2} \\ &= -\frac{4B_r}{1-B^2}, \end{aligned} \quad (132)$$

where $B_{\theta} = \frac{\partial B}{\partial \theta} = \frac{E_0 c \sin \theta}{2 \cosh^2(-\frac{E_0 c \cos \theta}{2})} e^{-\kappa_q(r-c)}$, $B_r = \frac{\partial B}{\partial r} = -\kappa_q B$.

Thus, it seems that we can calculate electric stress term $\rho \mathbf{E}$ from Eqs. (46) and (131). However, since we assume that the value of $\frac{\partial}{\partial \theta}$ is small enough, it is not appropriate to use Eq. (131) for the calculation of electric stress. Thus, we consider another method. That is, for the large voltage problem, we transform $F_0 \rho \mathbf{E}$ as follows:

$$\begin{aligned} F_0 \rho \mathbf{E} &= F_0 (-2c_q \sinh \phi_{\text{eq}}) [-\nabla(\phi_{\text{eq}} + \phi_f)] \\ &= \nabla(2F_0 c_q \cosh \phi_{\text{eq}}) + 2F_0 c_q \sinh \phi_{\text{eq}} \nabla \phi_f. \end{aligned} \quad (133)$$

Thus, by using the vector identity that $\text{rot grad} \equiv 0$, we obtain

$$T' = \hat{z} \cdot \text{rot}(F_0 \rho \mathbf{E}) = \hat{z} \cdot \text{rot}(2F_0 c_q \sinh \phi_{\text{eq}} \nabla \phi_f). \quad (134)$$

Therefore, we obtain velocity fields by the similar method described in Sec. IV (Model D).

Here, we define

$$\mathbf{B} = (B_r, B_{\theta}) \equiv 2F_0 c_q \sinh \phi_{\text{eq}} \nabla \phi_f, \quad (135)$$

where

$$B_r = 2F_0 E_0 c_q \left(1 - \frac{c^2}{r^2} \right) \sinh \phi_{\text{eq}} \cos \theta, \quad (136)$$

$$B_{\theta} = -2F_0 E_0 c_q \left(1 + \frac{c^2}{r^2} \right) \sinh \phi_{\text{eq}} \sin \theta. \quad (137)$$

Thus, we obtain

$$\begin{aligned} T' &= \frac{1}{r} \left[\frac{\partial}{\partial r} (r B_{\theta}) - \frac{\partial B_r}{\partial \theta} \right] \\ &= -2F_0 E_0 c_q \frac{\phi_{\text{eq}}}{\partial r} \left(1 + \frac{c^2}{r^2} \right) \cosh \phi_{\text{eq}} \sin \theta. \end{aligned} \quad (138)$$

Thus, by using $\frac{\phi_{\text{eq}}}{\partial r} = -2\kappa \sqrt{c_q} \sinh \frac{\phi_{\text{eq}}}{2}$, we obtain

$$T' = 4F_0 E_0 c_q^{\frac{3}{2}} \kappa \left(1 + \frac{c^2}{r^2} \right) \sinh \frac{\phi_{\text{eq}}}{2} \cosh \phi_{\text{eq}} \sin \theta, \quad (139)$$

$$= 2u_0 \frac{\kappa^3 c_q^{\frac{3}{2}}}{E_0 c} \left(1 + \frac{c^2}{r^2} \right) \sinh \frac{\phi_{\text{eq}}}{2} \cosh \phi_{\text{eq}} \sin \theta, \quad (140)$$

where

$$u_0 = 2F_0 E_0^2 c \epsilon^2. \quad (141)$$

By the change of valuable that $\kappa r = s$ and the replacement of T with T' , we transform Eq. (78) into

$$\kappa^4 \nabla_s^2 \Phi^{\text{st,eq}} = T', \quad (142)$$

where ∇_s^2 is a Laplacian for the valuable s . Thus, we obtain

$$\nabla_s^2 \Phi^{\text{st,eq}} = 2u_0 \frac{c_q^{3/2}}{E_0 c \kappa} \left(1 + \frac{c^2}{r^2}\right) \sinh \frac{\phi_{\text{eq}}}{2} \cosh \phi_{\text{eq}} \sin \theta = T'' \quad (143)$$

Further, since $u_\theta^{\text{large voltage}} = -\frac{\partial \Phi^{\text{st,eq}}}{\partial r} = -\kappa \frac{\partial \Phi^{\text{st,eq}}}{\partial s}$, we obtain

$$u_\theta^{\text{large voltage}} = -2I_0 u_0 \frac{c_q^{3/2}}{E_0 c} 2 \sin \theta, \quad (144)$$

where

$$I_0 = \frac{s}{2} \int_s^\infty \frac{\tilde{v}_p}{s'} ds' + \frac{1}{2s^3} \int_s^\infty s'^3 \tilde{v}_p ds', \quad (145)$$

$$\tilde{v}_p = -\frac{s^2}{4} \int_s^\infty \frac{\hat{T}''}{s'} ds' + \frac{1}{4s^3} \int_s^\infty s'^3 \hat{T}'' ds', \quad (146)$$

$$\hat{T}'' = \left(1 + \frac{c^2}{r^2}\right) \sinh \frac{\phi_{\text{eq}}}{2} \cosh \phi_{\text{eq}}. \quad (147)$$

E. Thickness of the ion-conserving area

We have a physical image on ion-conserving phenomena. That is, for small applied voltages, ion redistributions should occur at the most within an electrical double layer; thus, we expect that $d_{\text{eff}} = \epsilon$ (i.e., $f_e = d_{\text{eff}}/\epsilon = 1$) for the small applied voltages. Further, for larger applied voltages, this area should enlarge to compensate the shortage of ions. Thus, we can assume the nonlinear dependence of d_{eff} on v_0 ; however, unfortunately, we do not have a complete theory to determine d_{eff} and probably it is beyond the scope of this manuscript that clarifies ICEO phenomena mainly from the viewpoint of numerical simulation. Thus, from the numerical results by the FE-FV method, we determine

$$f_e(v_0) \equiv \frac{d_{\text{eff}}(v_0)}{\epsilon} = 1 + 3 \left(\frac{v_0}{40}\right)^{2.5}. \quad (148)$$

In more detail, we assume that $f_e(v_0) \equiv 1 + A_{e1} \left(\frac{v_0}{40}\right)^{B_{e1}}$ because physically we consider that $\lim_{v_0 \rightarrow 0} f_e = 1$ and we are interested in the behavior around $v_0 = 40$; then we determine the parameters as $A_{e1} = 3$ and $B_{e1} = 2.5$ from the curve fitting between the numerical results [circles in Fig. 8(a)] and the theoretical result of Eq. (144) [a solid line in Fig. 8(a)].

VI. THEORY (5): SIMPLE DC STEP RESPONSE THEORY BASED ON THE 2D POISSON-NERNST-PLANCK EQUATIONS

A. Surface charge and surface capacitance around a cylinder

By using the solution for the steady state [Eq. (55)], we can calculate a surface charge in an electrical double layer on the upper region of a circular cylinder [i.e., Region A;

$A = \{c \leq r \leq r_c, -\frac{\pi}{2} \leq \theta \leq \frac{\pi}{2}\}$] as follows:

$$\begin{aligned} q_A &\equiv \iint_A \rho dx dy \\ &= \int_{\theta=-\frac{\pi}{2}}^{\theta=+\frac{\pi}{2}} \int_{r=0}^{\infty} \frac{4E'_0 c}{K_1(\kappa r)} K_1(\kappa r) c \cos \theta dr d\theta \\ &\simeq 8E'_0 c^2 \epsilon = 4\tilde{\psi}_D c \epsilon \epsilon, \end{aligned} \quad (149)$$

where $r_c = c + d_{\text{eff}}$, $\tilde{\psi}_D = 2E'_0 c$, and a potential of outer edge of the electrical double layer is represented by $\psi_D = \tilde{\psi}_D \cos \theta$. Thus, by the definition of capacitance, the capacitance of the electrical double layer c_D is represented as

$$c_D^A \equiv \frac{dq_A}{d\tilde{\psi}_D} = 4\epsilon c. \quad (150)$$

It should be noted that we select r_c to be the position of just outside of the electrical double layer; however, we can replace r_c by “ ∞ ” in the integral of Eq. (149) since $K_1(\kappa r)$ becomes zero in the outside of the electrical double layer. Further, Eq. (149) is originally the equation for the steady state; however, by assuming the time-dependent surface potential of the outer edge of the double layer [$\tilde{\psi}_D(\tau) = 2E'_0(\tau)c$] with the boundary condition [$\tilde{\psi}_D = 2E_0 c$ at $\tau \rightarrow \infty$], we introduce the concept of the surface capacitance concerning Eq. (150).

B. Charging time of the cylinder for an unbounded problem

By using the PNP equations, especially, Eqs. (12) and (13), we obtain

$$\frac{\partial \rho}{\partial \tau} = \nabla_n \cdot (\nabla_n \rho + \bar{c} \nabla_n \phi), \quad (151)$$

where $\rho = c_+ - c_-$ and $\bar{c} = c_+ + c_-$. By integrating Eq. (151) over the surface region A, we obtain

$$\frac{\partial}{\partial \tau} \iint_A \rho dx dy = \iint_A \nabla_n \cdot (\nabla_n \rho + \bar{c} \nabla_n \phi) dx dy. \quad (152)$$

Thus, by using Gauss's divergence theorem and the definition of q_A , we transform Eq. (152) into

$$\frac{\partial q_A}{\partial \tau} = \int_{\bar{A}} (\nabla_n \rho + \bar{c} \nabla_n \phi) \mathbf{n} ds, \quad (153)$$

where \bar{A} is a surface of Region A, \mathbf{n} is surface normal unit vector, and $ds = r d\theta$ is a line element of \bar{A} . Further, since

$$\frac{\partial q_A}{\partial \tau} = \frac{\partial q_A}{\partial \tilde{\psi}_D} \frac{\partial \tilde{\psi}_D}{\partial \tau} = c_D^A \frac{\partial \tilde{\psi}_D}{\partial \tau} \quad (154)$$

and

$$\nabla_n \rho + \bar{c} \nabla_n \phi = 0 \left(\text{at } r = c, \text{ or } \theta = \pm \frac{\pi}{2} \right), \quad (155)$$

from Eq. (153) we obtain

$$c_D^A \frac{\partial \tilde{\psi}_D}{\partial \tau} = r_c \int_{-\frac{\pi}{2}}^{+\frac{\pi}{2}} \left(\frac{\partial \rho}{\partial r} + \bar{c} \frac{\partial \phi}{\partial r} \right) d\theta. \quad (156)$$

This is a fundamental equation for a charging time of the circular cylinder. Furthermore, since we can approximate

$r_c \simeq c$, $\bar{c} \simeq 2$, and $\frac{\partial \rho}{\partial r} \simeq 0$ at $r = r_c (\simeq c + \epsilon)$, we obtain that

$$c_D^A \frac{\partial \tilde{\psi}_D}{\partial \tau} \simeq 2 \int_{-\frac{\pi}{2}}^{+\frac{\pi}{2}} c \frac{\partial \phi}{\partial r} d\theta. \quad (157)$$

Here, in our physical understanding on ICEO, initially, the strength of the normal electric fields is $2E_0 \cos \theta$ from Eq. (41), and, finally, it becomes zero; at the same time, the potential of outer edge ψ_D becomes $2E_0 c \cos \theta$ in the final state from Eq. (34). Thus, it is reasonable to assume that

$$\left(c \frac{\partial \phi}{\partial r} \right)_{r=r_c} (\tau) \simeq [2E_0 c - \tilde{\psi}_D(\tau)] \cos \theta. \quad (158)$$

Thus, by using Eq. (158), we can transform Eq. (157) into

$$c_D^A \frac{\partial \tilde{\psi}_D}{\partial \tau} \simeq 2 \int_{-\frac{\pi}{2}}^{+\frac{\pi}{2}} (2E_0 c - \tilde{\psi}_D) \cos \theta d\theta = 4(2E_0 c - \tilde{\psi}_D). \quad (159)$$

Therefore, by using Eq. (150), we obtain

$$\frac{\partial \tilde{\psi}_D}{\partial \tau} = \frac{1}{\epsilon c} (2E_0 c - \tilde{\psi}_D). \quad (160)$$

Thus, we obtain

$$\tilde{\psi}_D = 2E_0 c \left[1 - \exp\left(-\frac{\tau}{\tau_A}\right) \right], \quad (161)$$

where

$$\tau_A = \epsilon c \quad (162)$$

and it is the charging time of the circular cylinder on ICEO for an unbounded problem.

C. Surface charge and surface capacitance on the parallel blocking electrodes for a bounded problem

For a bounded problem using the parallel blocking electrodes, we also need to consider the capacitance and charging time of the electrodes due to the formation of electrical double layers. Further, as the first step, we neglect the existence of the circular cylinder. In this case, by integrating ρ over Region B [= $\{0 \leq x \leq 0.5, 0 \leq y \leq L'_0\}$], we obtain

$$\begin{aligned} q_B &\equiv L'_0 \int_0^{0.5} \rho dx \\ &= -2\epsilon^2 L'_0 \int_0^{0.5} \frac{\partial^2 \phi}{\partial x^2} dx \\ &= -2\epsilon^2 L'_0 \left[\frac{\partial \phi}{\partial x} \right]_{x=0}^{x=0.5}, \end{aligned} \quad (163)$$

where $L'_0 (= 1.5)$ is a nondimensional width of the electrodes. Further, since $\frac{\partial \phi}{\partial x} = 0$ at $x = 0.5$ and $\frac{\partial \phi}{\partial x} = -2\kappa_q \sinh \frac{1}{2} \frac{v_0}{2}$ at $x = 0$ for a steady large voltage problem as discussed in 1D ion-conserving Poisson-Boltzmann theory [20], we obtain

$$q_B = -4\epsilon L'_0 \sqrt{c_q^B} \sinh \frac{\psi_D^B}{2}, \quad (164)$$

where $\psi_D^B (= 0.5v_0)$ is a double layer potential of the blocking electrode, $c_q^B = (-A' + \sqrt{1 + A'^2})^2$, and $A' =$

$2\epsilon \sinh^2(\psi_D^B/4)$. Thus, we define a surface capacitance on the blocking electrodes as

$$\begin{aligned} c_D^B &\equiv \frac{dq_B}{d\psi_D^B} \\ &= -2\epsilon L'_0 \left[\sqrt{c_q^B} \cosh \frac{\psi_D^B}{2} + \epsilon \left(\frac{A'}{\sqrt{1 + A'^2}} - 1 \right) \sinh^2 \frac{\psi_D^B}{2} \right]. \end{aligned} \quad (165)$$

However, as the first step, we just consider low voltage solutions that is consistent with Eqs. (149) and (150); i.e., for a steady small voltage problem (i.e., $c_q \simeq 1$ and $\sinh \psi_D^B/2 \simeq \psi_D^B/2$), the surface charge is

$$q_B \simeq -2\epsilon L'_0 \psi_D^B \quad (166)$$

and the surface capacitance

$$c_D^B \simeq -2\epsilon L'_0. \quad (167)$$

D. Charging time of the blocking electrodes for a bounded problem

Similarly to Sec. VI B, by integrating Eq. (151) over Region B, we obtain

$$\begin{aligned} c_D^B \frac{\partial \psi_D^B}{\partial \tau} &= L'_0 \int_0^{0.5} \frac{\partial}{\partial x} \left(\frac{\partial \rho}{\partial x} + \bar{c} \frac{\partial \phi}{\partial x} \right) dx \\ &= -L'_0 \left(\frac{\partial \rho}{\partial x} + \bar{c} \frac{\partial \phi}{\partial x} \right)_{x=0.5}, \end{aligned} \quad (168)$$

where we use a blocking electrode condition that $\frac{\partial \rho}{\partial x} + \bar{c} \frac{\partial \phi}{\partial x} = 0$ at $x = 0$. Thus, by using the approximations that $\bar{c} \simeq 2$ and $\frac{\partial \rho}{\partial x} \simeq 0$ at $x = 0.5$, we obtain

$$c_D^B \frac{\partial \psi_D^B}{\partial \tau} \simeq 2L'_0 \left(\frac{\partial \phi}{\partial x} \right)_{x=0.5}. \quad (169)$$

Here, in our physical understanding on an blocking electrode, a homogeneous electric field ($\frac{\partial \phi}{\partial x} = -v_0$) is initially appeared by the application of the voltage, and as the double layer potential (ψ_D^B) of the blocking electrode becomes larger the bulk electric field becomes smaller; thus, if the double layer is enough thin, we can assume that

$$\left(\frac{\partial \phi}{\partial x} \right)_{x=0.5} (\tau) \simeq -\frac{0.5v_0 - \psi_D^B(\tau)}{0.5}, \quad (170)$$

where the numerator ($0.5v_0 - \psi_D^B$) shows a bulk voltage and the denominator (0.5) shows the bulk distance of Region B. Therefore, by substituting Eqs. (167) and (170) into Eq. (169), we obtain

$$\frac{\partial \psi_D^B}{\partial \tau} = \frac{1}{0.5\epsilon} (0.5v_0 - \psi_D^B). \quad (171)$$

Thus, by using the conditions that $\psi_D^B = 0$ at $\tau = 0$ and $\psi_D^B = 0.5v_0$ at $\tau = \infty$, we obtain

$$\psi_D^B = 0.5v_0 \left[1 - \exp\left(-\frac{\tau}{\tau_B}\right) \right], \quad (172)$$

where

$$\tau_B = 0.5\epsilon \quad (173)$$

and it is the charging time of the blocking electrodes for a bounded problem.

E. Simple response model of an ICEO flow for an unbounded problem

We have already obtained the charging time $\tau_A (= \epsilon c)$ of the cylinder for the unbounded problem [Eq. (162)] and the time response equation [Eq. (161)]; i.e.,

$$\psi_D(\theta, \tau) = 2E_0 c g(\tau) \cos \theta,$$

where

$$g(\tau) = \left[1 - \exp\left(-\frac{\tau}{\tau_A}\right) \right].$$

Further, we can assume that $\phi_{\text{eq}} \propto \psi_D \propto g(\tau)$ since ψ_D is the potential of the outer edge of the electrical double layer. Thus, from Eq. (54), the time evolution of the equilibrium potential

ϕ_{eq} for an unbounded problem is described as

$$\phi_{\text{eq}}(\tau, r) = -\tilde{\phi}_{\text{eq}}(\tau, r) \cos \theta$$

with

$$\tilde{\phi}_{\text{eq}}(\tau, r) = 2E_0 c \frac{K_1(\kappa r)}{K_1(\kappa c)} g(\tau).$$

Therefore, from Eq. (B20) for Model B, the time evolution of the equilibrium slip velocity u_θ^{eq} is described as

$$u_\theta^{\text{eq}}(\tau) \simeq -u_0 \left(1 + \frac{c^2}{r^2} \right) \frac{\tilde{\phi}_{\text{eq}}(\tau, r)}{2E_0 c} \sin 2\theta.$$

Thus, we understand that $u_\theta^{\text{eq}} \propto \tilde{\phi}_{\text{eq}}(\tau, r) \propto g(\tau)$. Furthermore, by using the boundary condition that $u_\theta^f + u_\theta^{\text{eq}} = 0$ at $r = c$ with $u_\theta^f = 2C_2 r^3 \sin 2\theta$ [Eq. (73)], we obtain

$$u_\theta^f(\tau, r) \simeq 2u_0 \frac{c^3}{r^3} g(\tau).$$

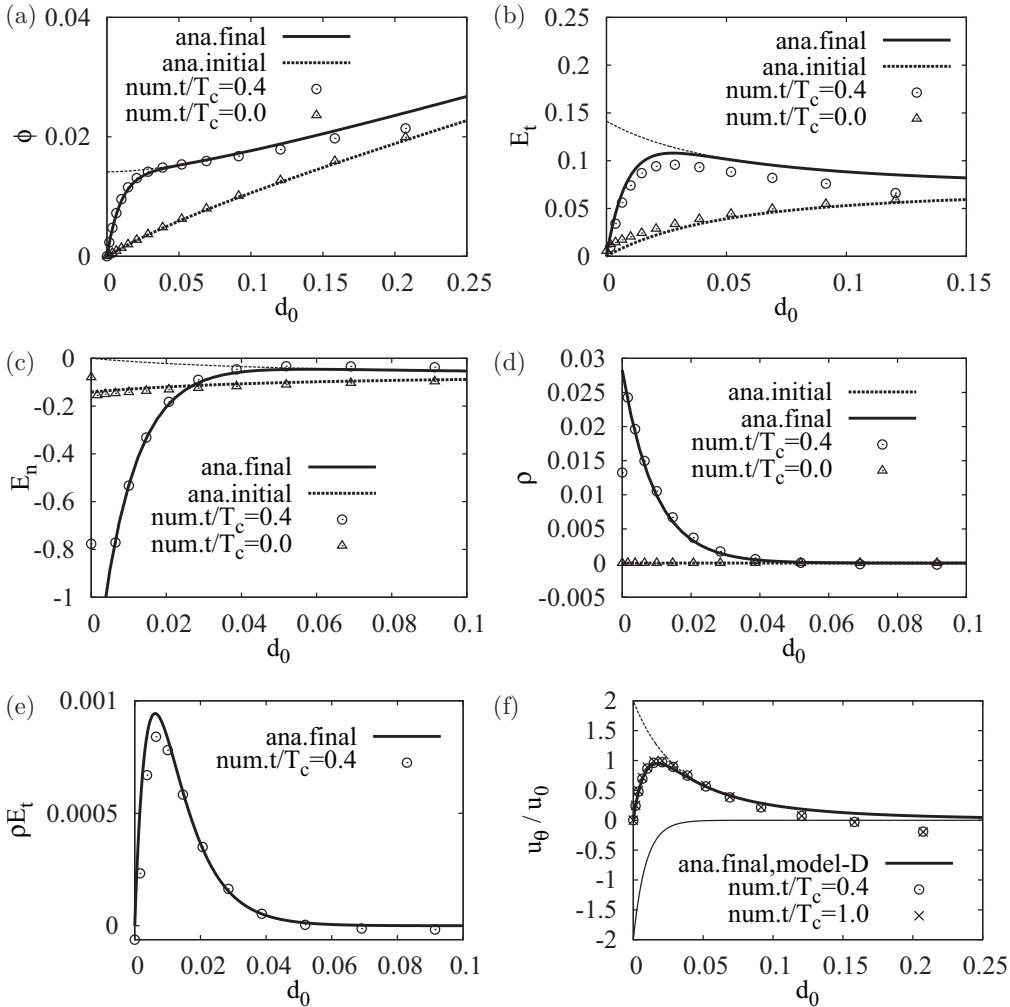


FIG. 3. Comparison between the numerical and analytical results for an unbounded problem at $\kappa = 100$, $v_0 = 0.1$, $c = 0.1$, and $\theta = 45^\circ$. (a)–(f) show the dependence of the potential, tangential electric field, normal electric field, charge density, tangential electric force, and tangential flow velocity, respectively, on the surface distance. Here the triangles, circles, and crosses show the numerical results obtained by use of the FE-FV method at $t/T_c = 0, 0.4$, and 1.0 , respectively; the thick broken and solid lines show the analytical results obtained by use of the small voltage theory for the initial and final states, respectively, while the thin broken and solid lines show the analytical results for the outer and inner solutions, respectively, at the final state.

Since $u_\theta(\tau, r) = u_\theta^f(\tau, r) + u_\theta^{\text{eq}}(\tau, r)$, we obtain that

$$\begin{aligned} u_\theta^{\text{unbounded}}(\tau, r) &\simeq 2u_0 \frac{c^3}{r^3} g(\tau) - u_0 \left(1 + \frac{c^2}{r^2}\right) \frac{\tilde{\phi}_{\text{eq}}(\tau, r)}{2E_0 c} \sin 2\theta \\ &= 2u_0 \left[\frac{c^3}{r^3} - \left(1 + \frac{c^2}{r^2}\right) \frac{K_1(\kappa r)}{2K_1(\kappa c)} \right] g(\tau) \sin 2\theta. \end{aligned}$$

Namely, we also understand that $u_\theta \propto g(\tau)$. Therefore, to more simply explain the time evolution of the maximum velocity in the direction of θ around a cylinder for an unbounded problem, we can propose a simple model that considers the growing double layer with the time constant τ_A as follows:

$$\begin{aligned} u_\theta^{\text{max, unbounded}}(v_0, \kappa, \theta, \tau) \\ = u_\theta^{\text{max, steady, } \theta=45^\circ}(v_0, \kappa) \left[1 - \exp\left(-\frac{\tau}{\tau_A}\right) \right] \sin 2\theta, \quad (174) \end{aligned}$$

where $\tau_A = \epsilon c$ and $u_\theta^{\text{max, steady, } \theta=45^\circ}$ is the maximum velocity in the direction of θ ($= 45^\circ$) in a steady state; further,

$u_\theta^{\text{max, steady, } \theta=45^\circ}$ is calculated by the method described in Sec. IV and V for small and large voltages.

It should be noted that one of the reasonable approaches seems to be to consider the Helmholtz-Smoluchowski formula

$$\mathbf{u}_d = -\frac{\epsilon \zeta}{\mu} \mathbf{E}_\theta$$

with the assumptions that $\zeta \propto g(\tau)$ and $\mathbf{E}_\theta \propto g(\tau)$ [13]. However, unfortunately, the result of this approach [$u_\theta \propto g(\tau)^2$] could not explain the numerical results of the time response of u_θ^{max} at all. Thus, we soon understand that we need to consider this problem more precisely; fortunately, our theories in Sec. II to VI and Appendix B suggest a more precise solution as mentioned before.

F. Simple response model of an ICEO flow for a bounded problem

We have already obtained the charging time τ_B ($= 0.5\epsilon$) of the electrical double layer of the blocking electrodes [in

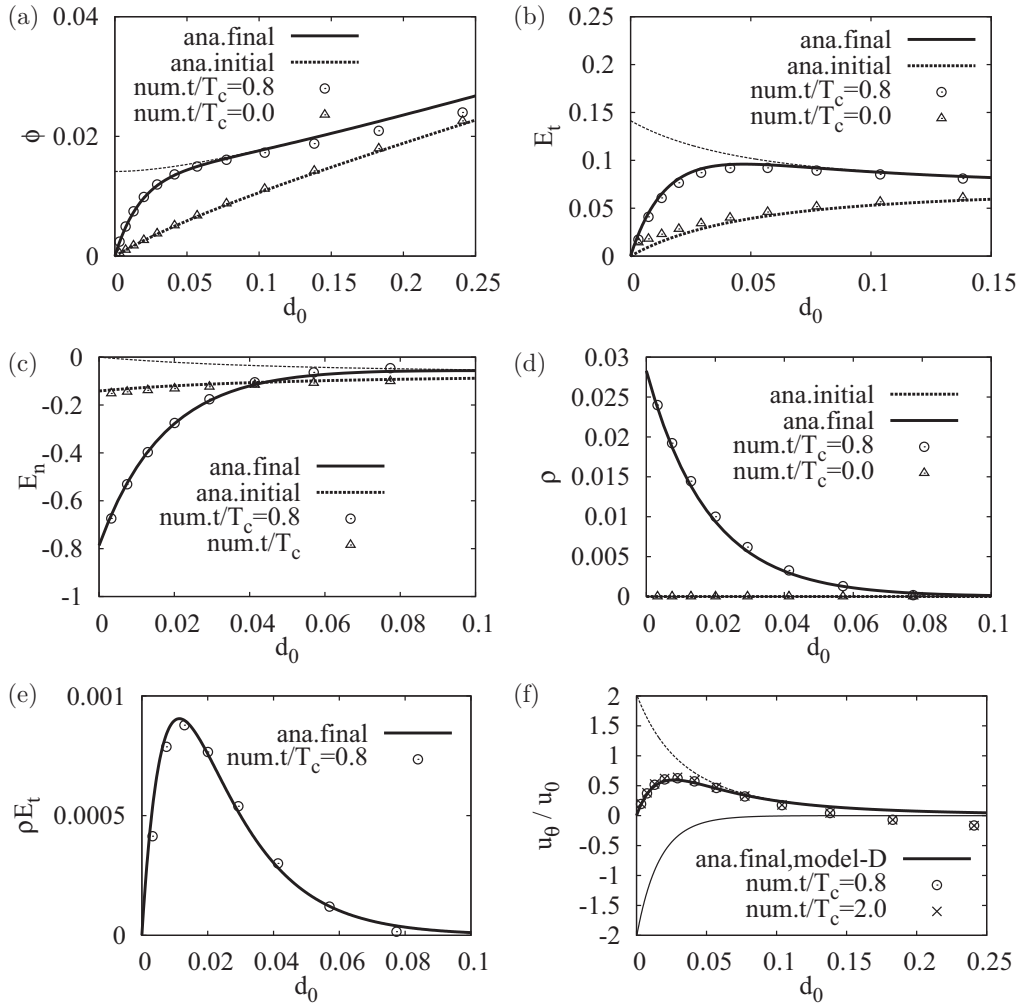


FIG. 4. Comparison between the numerical and analytical results for an unbounded problem at $\kappa = 50$, $v_0 = 0.1$, $c = 0.1$, and $\theta = 45^\circ$. (a)–(f) show the dependence of the potential, tangential electric field, normal electric field, charge density, tangential electric force, and tangential flow velocity, respectively, on the surface distance. Here the triangles, circles, and crosses show the numerical results obtained by the FE-FV method at $t/T_c = 0, 0.8$, and 2.0 , respectively; the thick broken and solid lines show the analytical results obtained by the small voltage theory for the initial and final states, respectively, while the thin broken and solid lines show the analytical results obtained by the small voltage theory for the outer and inner solutions, respectively, at the final state.

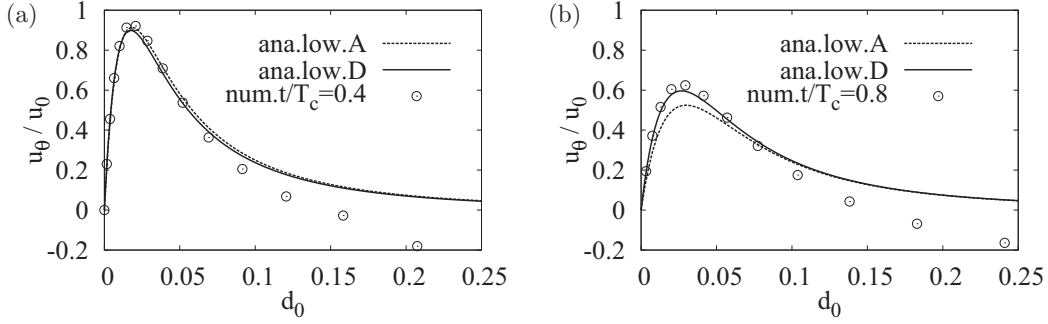


FIG. 5. Comparison between Model A and Model D for an unbounded problem at $v_0 = 0.1$ and $c = 0.1$. (a) and (b) show the dependence of u_θ on d_0 at $\kappa = 100$ and 50 , respectively. Here, Model D [solid line obtained by Eq. (97)] is a full analytical model that describes a finite double-layer structure, whereas Model A [broken line obtained by Eq. (B11)] is a simple model that is just justified in the limit of a thin-double-layer approximation, as described in Sec. III and Appendix B; further, the circles in (a) and (b) show the numerical results obtained by use of the FE-FV method described in Sec. II and Appendix A at $t/T_c = 0.4$ and 0.8 , respectively.

Eq. (173)] and the time response equation on the potential of the blocking electrodes ψ_D^B for the unbounded problem [in Eq. (172)], i.e.,

$$\psi_D^B(\tau) = 0.5v_0[1 - g_B(\tau)],$$

where

$$g_B(\tau) = \exp\left(-\frac{\tau}{\tau_A}\right).$$

Obviously, ϕ^{eq} decays by the factor $g_B(\tau)$. Thus, similarly to the previous problem, the time evolution of the equilibrium potential ϕ_{eq} for a bounded problem is described from Eq. (54) as

$$\phi_{\text{eq}}(\tau, r) = -\tilde{\phi}_{\text{eq}}^B(\tau, r) \cos \theta$$

with

$$\tilde{\phi}_{\text{eq}}^B(\tau, r) = 2E_0c \frac{K_1(\kappa r)}{K_1(\kappa c)} g(\tau) g_B(\tau).$$

Therefore, from Eq. (B20) for Model B, the time evolution of the equilibrium slip velocity u_θ^{eq} for a bounded problem is described as

$$u_\theta^{\text{eq}}(\tau) \simeq -u_0 \left(1 + \frac{c^2}{r^2}\right) \frac{\tilde{\phi}_{\text{eq}}^B(\tau, r)}{2E_0c} \sin 2\theta.$$

Thus, we understand that $u_\theta^{\text{eq}} \propto \tilde{\phi}_{\text{eq}}^B(\tau, r) \propto g(\tau)g_B(\tau)$. Further, by using the boundary condition that $u_\theta^f + u_\theta^{\text{eq}} = 0$ at $r = c$ with $u_\theta^f = 2C_2r^3 \sin 2\theta$ [Eq. (73)], we obtain

$$u_\theta^f(\tau, r) \simeq 2u_0 \frac{c^3}{r^3} g(\tau) g_B(\tau).$$

Since $u_\theta(\tau, r) = u_\theta^f(\tau, r) + u_\theta^{\text{eq}}(\tau, r)$, we obtain that

$$\begin{aligned} u_\theta^{\text{bounded}}(\tau, r) &\simeq 2u_0 \frac{c^3}{r^3} g(\tau) - u_0 \left(1 + \frac{c^2}{r^2}\right) \frac{\tilde{\phi}_{\text{eq}}^B(\tau, r)}{2E_0c} \sin 2\theta \\ &= 2u_0 \left[\frac{c^3}{r^3} - \left(1 + \frac{c^2}{r^2}\right) \frac{K_1(\kappa r)}{2K_1(\kappa c)} \right] g(\tau) g_B(\tau) \sin 2\theta. \end{aligned}$$

Namely, we understand that $u_\theta^{\text{bounded}} \propto g(\tau)g_B(\tau)$. Therefore, more simply to explain time evolution of the maximum velocity in the direction of θ around a cylinder for a bounded problem using blocking electrodes, we can propose a simple model that considers the growing and decaying double layer with the time constants τ_A and

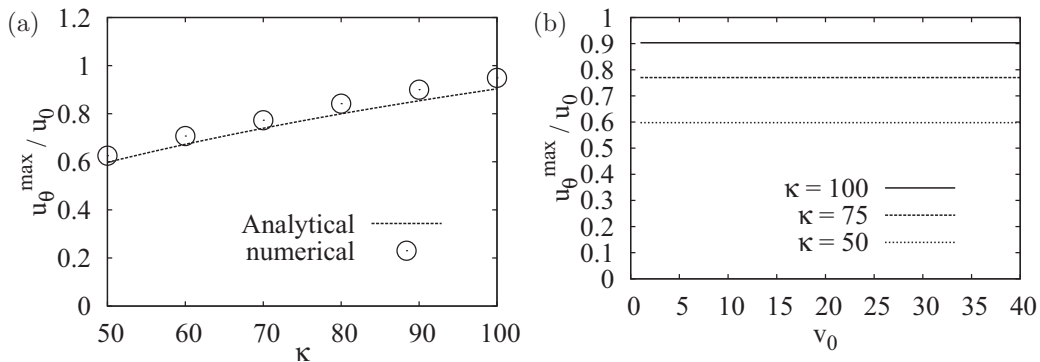


FIG. 6. Dependence of u_θ^{max} on κ and v_0 for an unbounded problem at $c = 0.1$ and $\theta = 45^\circ$. (a) Dependence of u_θ^{max} on κ at $v_0 = 0.1$. (b) Dependence of u_θ^{max} on v_0 . In (a) the broken line shows the analytical results predicted by the small voltage theory [Eq. (97)] on $v_0 = 0.1$, while the circles show the numerical results calculated by the FE-FV method at $v_0 = 0.1$. In (b) the solid, dashed, and broken lines show the analytical results predicted by the small voltage theory [Eq. (97)] at $\kappa = 100, 75,$ and 50 , respectively.

τ_B as follows:

$$\begin{aligned}
 u_\theta^{\max, \text{bounded}}(v_0, \kappa, \theta, \tau) \\
 = u_\theta^{\max, \text{steady}, \theta=45^\circ}(v_0, \kappa) \left[1 - \exp\left(-\frac{\tau}{\tau_A}\right) \right] \\
 \times \exp\left(-\frac{\tau}{\tau_B}\right) \sin 2\theta, \quad (175)
 \end{aligned}$$

where $\tau_A = \epsilon c$ and $\tau_B = 0.5\epsilon$.

VII. RESULTS

A. dc step responses of ICEO flows for an unbounded problem at small applied electric fields

Figures 2(a)–2(c) show the time evolution of flow fields by use of the multiphysics calculation method (FE-FV method) when a small sudden electric field ($E_0 = v_0 = 0.1$) is applied for an unbounded problem under the conditions that $c = 0.1$ and $\kappa = 100$. As shown in Figs. 2(a), 2(b), and 2(c), we observe small, moderate, and maximum quadrupolar vortex flows around a cylinder at $t/T_c = 0.02$, 0.1, and 0.4, respectively. Figure 2(d) shows the time dependence of the maximum velocity u_θ^{\max} in the direction of $\theta (= 45^\circ)$. Here, the circles and squares (the solid and broken lines) show the numerical (analytical) results at $\kappa = 100$ and 50, respectively. As shown in Fig. 2(d), the analytical results obtained by the simple response model described in Sec. VI agree well with the numerical results by use of the FE-FV method. Thus, we find that the small quadrupolar vortices due to the motion of ions are generated from the early stage; further, they grow

during the charging time of the cylinder (τ_A) and the velocity becomes the maximum velocity (of the steady state) predicted by Eq. (98) of the small voltage theory.

B. Comparison between the numerical and analytical results for an unbounded problem at small applied electric fields

Figures 3 and 4 show the comparison between the numerical and analytical results for an unbounded problem at $\kappa = 100$ and 50, respectively, at $E_0 = v_0 = 0.1$ and $c = C_d/W_0 = 0.1$. More specifically, Figs. 3(a)–3(f) [Figs. 4(a)–4(f)] show the dependence of ϕ , E_r , E_θ , ρ , ρE_θ , and u_θ , respectively, on the surface distance d_0 at $\kappa = 100$ ($\kappa = 50$) and $\theta = 45^\circ$. Here, in Fig. 3 (Fig. 4), the triangles, circles, and crosses show the numerical results obtained by use of the FE-FV method described in Sec. II and Appendix A at $t/T_c = 0, 0.4$, and 1.0, respectively (at $t/T_c = 0, 0.8$, and 2.0, respectively); further, the thick broken and solid lines (thin broken and solid lines) show the analytical results obtained by use of the small voltage theory described in Secs. III and IV for the initial and final states, respectively (for the outer and inner solutions, respectively, at the final state). As shown in Figs. 3 and 4, the numerical results agree well with the analytical results in the initial and steady states. Thus, the reliability of our simulator and the FE-FV method are examined. Further, as shown in Fig. 3(f) [Fig. 4(f)], the value of $u_{\theta, f}$ (thin broken line) decreases proportionally to $\frac{1}{r^3}$ as predicted in Eq. (73), while the value of $u_{\theta, \text{eq}}$ (thin solid line) increases with a characteristic length $1/\kappa$. Furthermore, Figs. 5(a) and 5(b) show the comparison between Model A and Model D for an unbounded problem at $\kappa = 100$ and

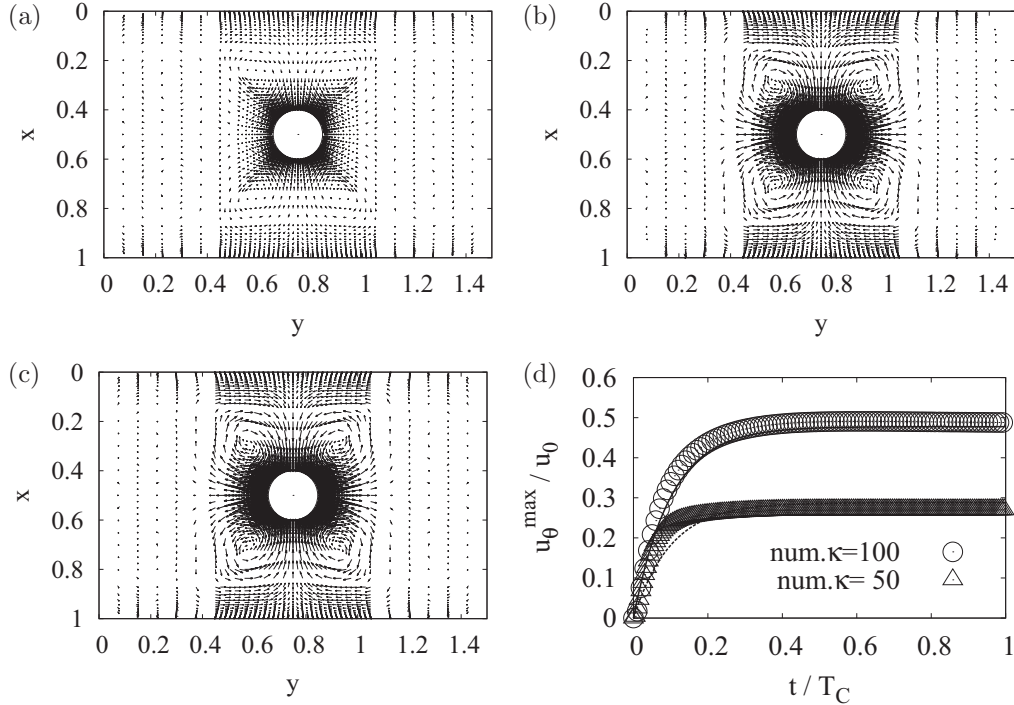


FIG. 7. Time evolution of ICEO flow fields for an unbounded problem at large applied electric fields ($E_0 = v_0 = 40$). (a), (b), and (c) show the flow fields at $t/T_c = 0.02$, 0.40, and 1.00, respectively, at $\kappa = 100$ and $c = 0.1$. (d) shows the dependence of u_θ^{\max} on t at $v_0 = 40$ and $c = 0.1$; in (d), the solid and broken lines show the analytical results obtained by Eq. (174) with Eq. (144) at $\kappa = 100$ and 50, respectively, while the circles and triangles show the numerical results by use of the FE-FV method at $\kappa = 100$ and 50, respectively.

50, respectively. Here, Model D is a full analytical model that describes a finite double-layer structure, whereas Model A is a simple model that is just justified in the limit of a thin-double-layer approximation, as described in Sec. III and Appendix B. However, the results of Model A surprisingly agrees with those of Model D at $\kappa = 100$, while the results of Model A slightly differ from those of Model D at $\kappa = 50$, as shown in Fig. 5.

Figures 6(a) and 6(b) show the dependence of u_θ^{\max} on κ and v_0 , respectively, for an unbounded problem at a small voltage ($v_0 = 0.1$). Here the lines show analytical results predicted by a small voltage theory, while the circles show the numerical results calculated by use of the FE-FV method. As shown in Fig. 6(a), the numerical results agree well with the analytical results, and the maximum surface velocity (u_θ at $\theta = 45^\circ$) becomes larger as κ becomes larger. This is because the peak position is shifted to the smaller value of d_0 by using larger κ , while the absolute value of $u_{\theta,f}(= -u_{\theta,eq})$ at $r = c$ is considered to be $2u_0$. Thus, the maximum surface velocity becomes larger as κ becomes larger. Figure 6(b) shows the predictions of the dependence of u_θ/u_0 on v_0 at $\kappa = 100, 75$, and 50 by the small voltage theory. As shown in Fig. 5(b), in the small voltage theory, u_θ is proportional to u_0 , and thus u_θ is proportional to v_0^2 completely. However, as mentioned later, we need to correct this prediction a little for large voltages.

C. dc step responses of ICEO flows for an unbounded problem at large voltages

Figures 7(a)–7(c) show the time evolution of flow fields by use of the multiphysics calculation method (FE-FV method)

when a large sudden electric field ($E_0 = v_0 = 40$) is applied for an unbounded system under the conditions that $c = 0.1$ and $\kappa = 100$. As shown in Figs. 7(a)–7(c), we also observe the growing of quadrupolar vortex flows around a cylinder from $t/T_c = 0.02$ to 0.4, and we observe the steady state from $t/T_c = 0.4$ to 1.0. Figure 7(d) shows the time dependence of the maximum velocity u_θ^{\max} in the direction of $\theta (= 45^\circ)$. Here the circles and triangles (solid and broken lines) show the numerical (analytical) results at $\kappa = 100$ and 50, respectively. As shown in Fig. 7(d), the analytical results obtained by the simple response model with the large voltage theory of Sec. V agree fairly well with the numerical results by use of the FE-FV method, although we find a slight difference for the results at $\kappa = 50$. Thus, our simple response theory is valid for the wide range of applied voltages at least in the limit of a thin electrical double layer.

D. Comparison between the numerical and analytical results for an unbounded problem at large applied electric fields

Figure 8 shows the dependence of u_θ^{\max} on κ and v_0 for an unbounded system at a large applied electric field. In Figs. 8(a) and 8(b), the thick solid line and circles show the analytical results predicted by the large voltage theory and the numerical results calculated by use of the FE-FV method, respectively, while the thin solid line shows the analytical results predicted by the small voltage theory. As shown in Figs. 8(a) and 8(b), the numerical results agree well with the analytical results predicted by the large voltage theory that assumes $f_e = f_v = 1 + 3(\frac{v_0}{40})^{2.5}$ and disagree with the predictions by the small

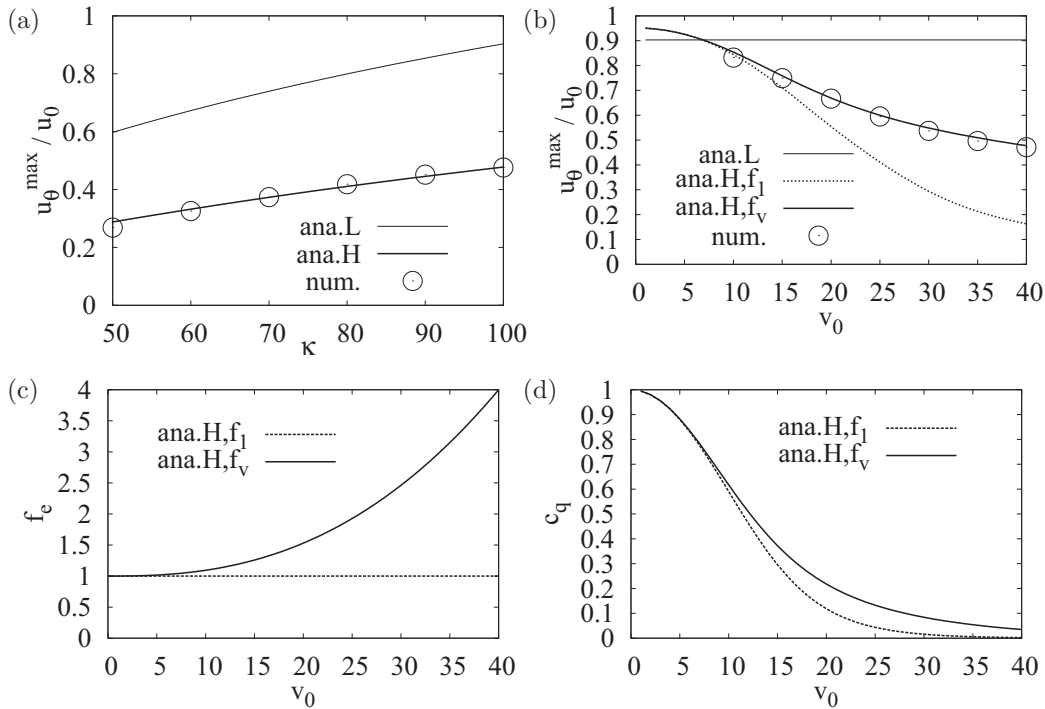


FIG. 8. Dependence of u_θ^{\max} on κ and v_0 for an unbounded system at a large applied electric field at $\theta = 45^\circ$ and $c_0 = 0.1$. (a) Dependence of u_θ on κ at $v_0 = 40$. (b) Dependence of u_θ on v_0 at $\kappa = 100$. (c) Dependence of $f_e (= d_{\text{eff}}/\epsilon)$ on v_0 at $\kappa = 100$. (d) Dependence of c_q on v_0 at $\kappa = 100$. In (a) and (b), the thick and thin solid lines show the analytical results predicted by the large and small voltage theory, respectively, while the circles show the numerical results calculated by use of the FE-FV method. In (b), (c), and (d) the thick solid and thick broken lines show the analytical results predicted by the large voltage theory [Eq. (144)] with $d_{\text{eff}}(v_0) = \epsilon + 3\epsilon(\frac{v_0}{40})^{2.5}$ and ϵ , respectively.

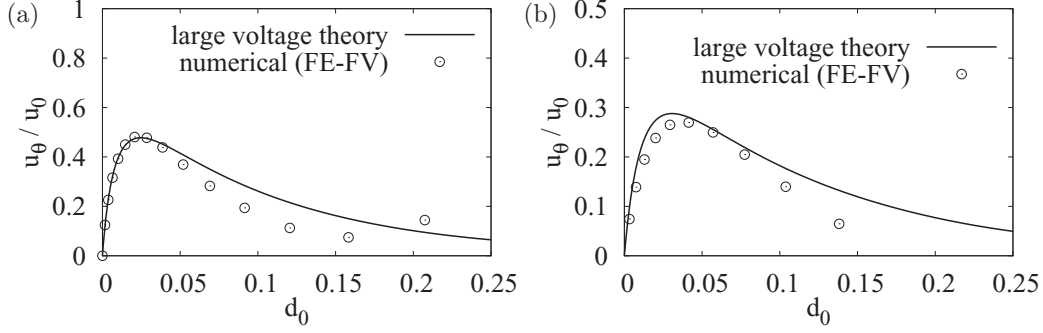


FIG. 9. Flow fields for an unbounded problem in the electrical double layer at a large applied field ($E_0 = v_0 = 40$). (a) and (b) show the dependence of the tangential flow velocity on d_0 at $\kappa = 100$ and 50 , respectively, at $\theta = 45^\circ$ and $c_0 = 0.1$. Here, the circles show the numerical results obtained by use of the FE-FV method, while the lines show the analytical results obtained by use of Eq. (144). As shown in (a) and (b), the analytical and numerical results agree fairly well.

voltage theory. Further, in Fig. 8(b), the broken line shows the prediction when we assume that $f_e = f'_1 = 1$ (i.e., $d_{\text{eff}} = \epsilon$) in the large voltage theory. As shown in Fig. 8(b) the broken line does not agree with the numerical results. Thus, to explain numerical results obtained by use of the FE-FV method, we need to introduce nonlinearity for the effective factor f_e , as shown in Fig. 8(c). Further, in Fig. 8(d), the broken and solid lines show the dependence of c_q on d_0 corresponding to $f_e = f'_1$ and f_v , respectively. Furthermore, Fig. 9 shows the flow fields at a large voltage ($v_0 = 40$). Here, the circles and solid line show the numerical and analytical results. As shown in Fig. 9, the numerical results at $\kappa = 100$ agree fairly well with the analytical results, while the numerical results at $\kappa = 100$ differs a bit from the analytical results even for the increasing

slope. This is because, rigorously, our large voltage theory is valid only for the thin-double-layer limit.

E. Complex phenomena due to flow effects for an unbounded problem at large applied fields

The ICEO phenomena at large voltages are a little more complex than expected. Namely, numerical calculations show that the distributions of $\rho(d_0)$ and $E_r(d_0)$ at different values of θ at the early stage ($t/T_c = 0.02$) differ, as shown in Figs. 10(a) and 10(c); however, their distributions at the final stage ($t/T_c = 1$) almost become the same, as shown in Figs. 10(b) and 10(d). This behavior differs from our analytical theory in Sec. V and the distributions are explained by the theory at

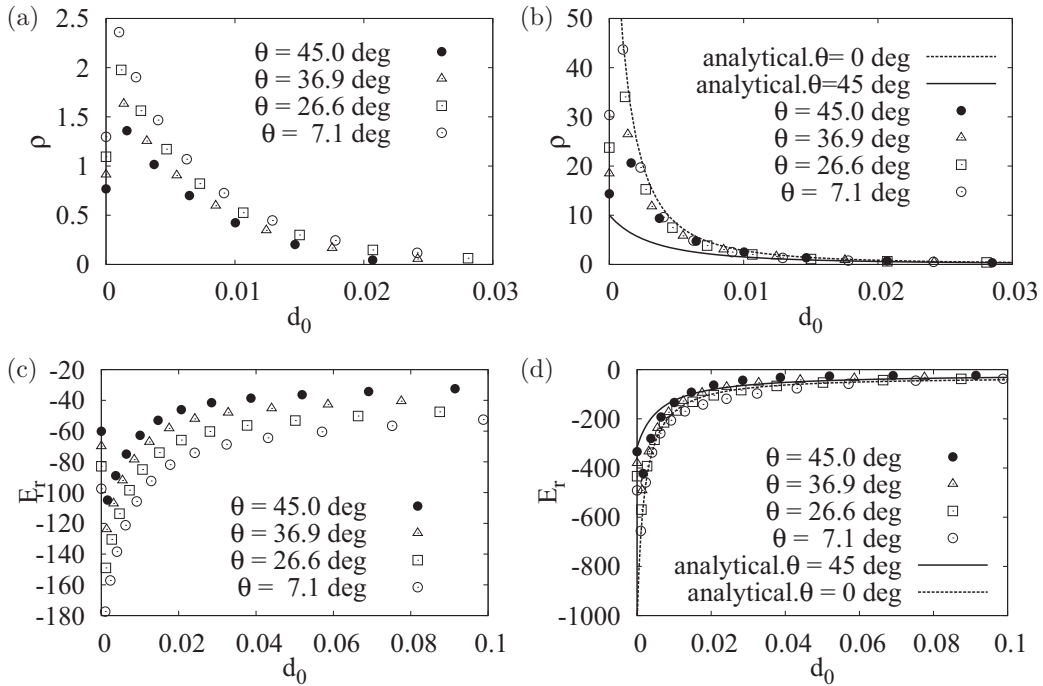


FIG. 10. Complex phenomena due to flow effects on the distributions of ρ and E_r for an unbounded system. (a) and (b) [(c) and (d)] show the dependence of ρ (E_r) on d_0 at $t/T_c = 0.02$ and 1.00 , respectively. Here, $E_0 = v_0 = 40$, $\kappa = 100$, and $c = 0.1$; the closed circles, triangles, squares, and open circles show the numerical results by use of the FE-FV method at $\theta = 45.0^\circ$, 36.9° , 26.6° , and 7.1° , respectively, while the solid and broken lines show the analytical results obtained by use of the large voltage theory in Sec. V [i.e., $\rho = -2c_q \sinh \phi_{\text{eq}}$ and $E_r = E_r^f + E_r^{\text{eq}}$ with Eqs. (35) and (132)] at $\theta = 45^\circ$ and 0° , respectively.

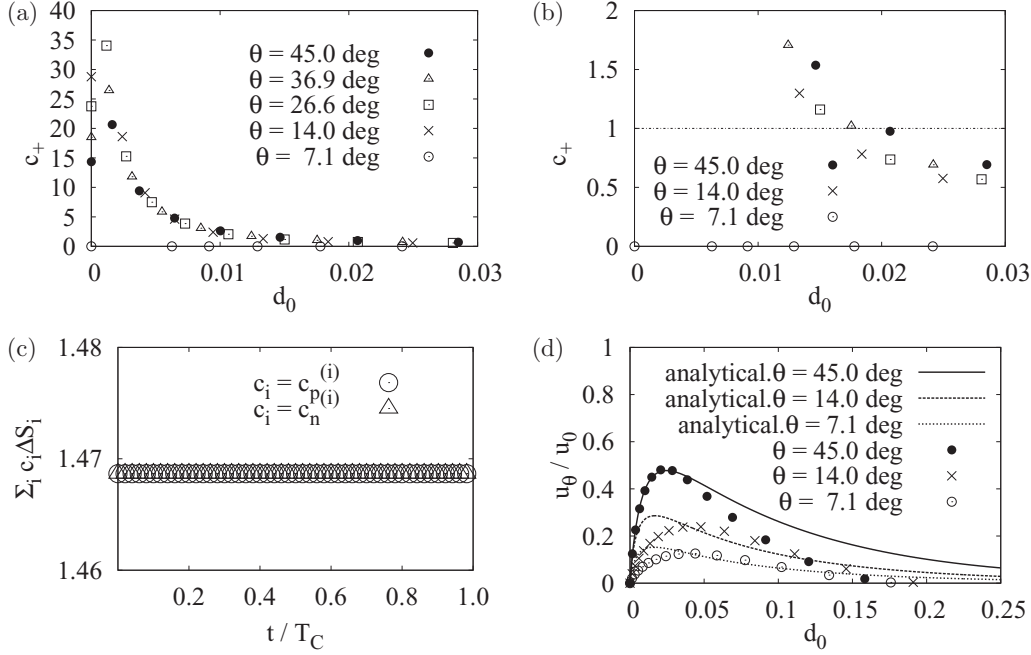


FIG. 11. Complex phenomena due to flow effects on the distributions of ions for an unbounded system. (a) and (b) show the ion distributions in the large and small concentration ranges, respectively, at $t/T_c = 1$; (c) shows the dependence of the total ion numbers on t and (d) shows the dependence of u_θ on d_0 ; $v_0 = 40$, $\kappa = 100$, and $c = 0.1$. In (a), (b), and (d), the closed circles, triangles, squares, crosses, and open circles show the numerical results by use of the FE-FV method at $\theta = 45.0^\circ$, 36.9° , 26.6° , 14.0° , and 7.1° , respectively. In (d), the solid, dashed, and broken lines show the analytical results obtained by Eq. (144) at $\theta = 45.0^\circ$, 14.0° , and 7.1° , respectively. As shown in (c), the total ion numbers are preserved completely without the use of any scaling algorithm.

$\theta = 0^\circ$ rather than the theory at $\theta = 45^\circ$ as shown in Figs. 10(b) and 10(d). We believe that this is due to a flow effect (on ion distributions) that we neglect in our analytical theory; i.e., once a flow is generated in the electrical double layer, the laminar flow forces the distributions of ρ and E_r to be almost the same.

Figures 11(a) and 11(b) show the distributions of the concentration of a positive ion in the large and small ranges, respectively, at $\theta = 45.0^\circ$, 36.9° , 26.6° , 14.0° , and 7.1° . As shown in Fig. 11(a), the surface concentration of the ions near the surface of the cylinder increases because of the large applied voltage ($t/T_c = 1$); however, it never exceeds the steric limit, even at large applied voltages. Thus, in our calculations, we need not consider the steric effect and ion crowding effect. Further, as shown in Fig. 11(b), the value of c_+ outside of the diffused ion region is smaller than 1 at large applied voltages; i.e., the ions are exhausted because of the ion-conserving effects at large applied voltages. Figure 11(c) shows the time dependence of the total ion numbers calculated from $\sum_i c_i \Delta S_i$, where c_i ($c_+^{(i)}$ or $c_-^{(i)}$) and ΔS_i denote an ion concentration and an area of the i -th element, respectively. As shown in Fig. 11(c), the total ion numbers are preserved completely without the use of any scaling algorithm. Thus, the ion-conserving condition and the flow effect on ion distributions play an important role in the decrease of an ICEO flow strength at large applied voltages. In addition, because of the flow effect, distributions of u_θ are not explained by the large voltage theory except at $\theta = 45^\circ$, as shown in Fig. 10(e), although they are rather explained by the simple theory that $u_\theta = u_\theta^{\max} \sin 2\theta$.

F. dc step responses of ICEO flows for a bounded problem using the finite-distance blocking electrodes at large voltages

Figures 12(a) to 12(c) show the time evolution of flow fields by use of the multiphysics calculation method (FE-FV method) when a large sudden electric field ($E_0 = v_0 = 40$) is applied for a bounded system using the finite-distance blocking electrodes, under the conditions that $c = 0.1$ and $\kappa = 100$. As shown in Figs. 12(a), 12(b), and 12(c), we observe small, maximum, and small quadrupolar vortex flows around a cylinder at $t/T_c (= Dt/W_0\lambda_D) = 0.02$, 0.18, and 1, respectively. Figure 12(d) shows the time dependence of the surface maximum velocity (u_θ^{\max} at $\theta = 45^\circ$). As shown in Fig. 12(d), the analytical results obtained by the simple response theory (in Sec. VI) [Eq. (175) with Eq. (144)] agree very well with the numerical results by use of the FE-FV method. Thus, for the bounded system using the blocking electrode, we find that small quadrupolar vortices due to the motion of ions are also generated from the early stage; further, they grow during the charging time of the cylinder and decay during the charging time of the parallel electrodes.

VIII. DISCUSSION

A. Observable peak velocities on ICEO in a dilute electrolyte (<0.1 mM)

Our theory clarifies that an observable peak velocity on ICEO is not $2u_0$ but approximately $0.9u_0$ at $\kappa = 100$ at small applied voltages, as shown in Fig. 6(b), because of

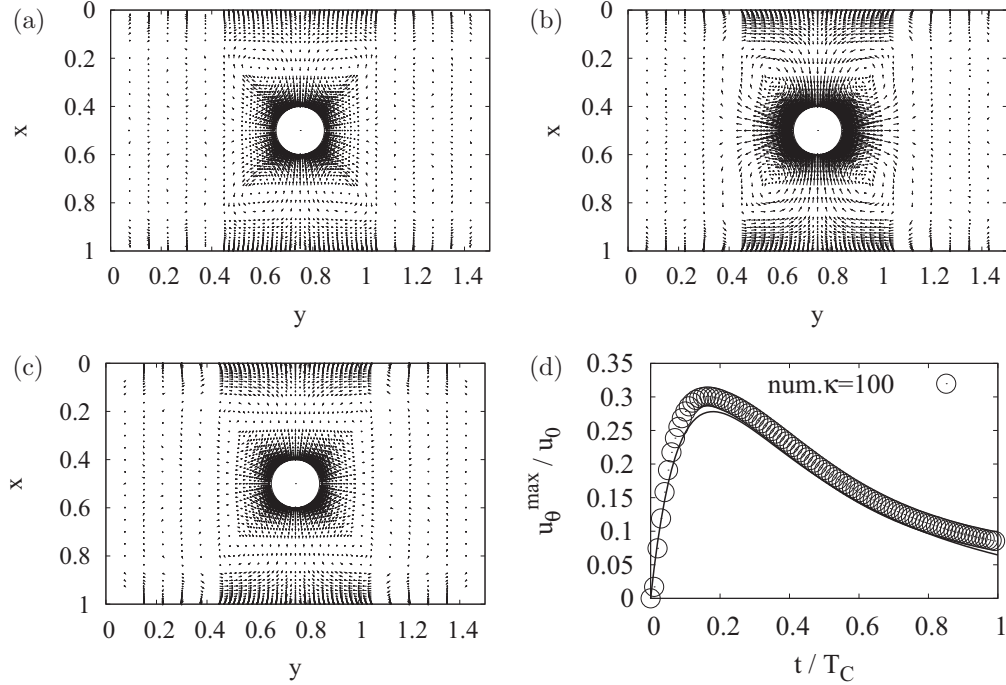


FIG. 12. Time evolution of ICEO flow fields for a bounded problem using the finite-distance blocking electrodes at a large applied electric field ($E_0 = v_0 = 40$). (a), (b), and (c) show the flow fields at $t/T_C = 0.02$, 0.18 , and 1.00 , respectively, at $\kappa = 100$ and $c = 0.1$. (d) shows the dependence of u_θ^{\max} on t at $v_0 = 40$ and $c = 0.1$; in (d), the solid line shows the analytical results obtained by Eq. (175) with Eq. (144), while the circles show the numerical results by use of the FE-FV method.

the boundary condition that $u_\theta = 0$ on the cylinder. Please note that the conventional value $2u_0$ is a virtual limit on the conductive surface for the outside solution [i.e., $u_\theta^f(c)$] and it does not mean the observable peak velocity in ICEO experiments (u_θ^{peak}). Further, because of large voltage effects explained by the 2D ion-conserving Poisson-Boltzmann theory, the observable peak velocity on ICEO decreases to the level of $0.5u_0$, as shown in Fig. 8(b), at $\kappa = 100$ and $v_0 = 40$; e.g., $V_0 = 1\text{ V}$, $W = 100\ \mu\text{m}$, and $E = 10\ \text{kV/m}$. Namely, the observable peak velocities in the ICEO experiments are expected to be just 25% of the standard prediction ($2u_0$).

This new insight greatly helps our understandings on ICEO since the maximum flow velocities on ICEO in the experiments are often much smaller than the standard predictions as summarized in Ref. [3]. For example, Levitan *et al.* [22] measured the maximum slip velocity around a platinum wire of radius $50\ \mu\text{m}$ at $E = 10\ \text{kV/m}$ in a dilute KCl solution ($<0.1\ \text{mM}$) and fitted their theoretical predictions to the experimental data by assuming the correction factor $\Lambda = 1/(1 + \delta)$ and $\delta = 1.5$; i.e., $\Lambda = 0.4$. Further, Hanett *et al.* [8] also measured ICEO flow velocities around a gold-coated circular post of radius $75\ \mu\text{m}$ at $E \simeq 10\ \text{kV/m}$ in a $0.1\ \text{M}$ solution and fitted their theoretical predictions to their experimental data by assuming $\Lambda = 0.25$. Furthermore, for coplanar microelectrodes in a KCl solution ($0.16\ \text{mM}$), Green *et al.* [23] measured ACEO slip velocities and obtained $\Lambda = 0.25$. As a whole, our predictions at large voltages seems to be reasonable to explain experimental results for a small characteristic length ($c_d < 100\ \mu\text{m}$) in dilute solution ($C_0 < 0.1\ \text{mM}$), although we may need more systematic research in experiments and calculations.

B. Usefulness of a thin-double-layer approximation

Although we claimed that $2u_0$ is not an observable peak value, of course, it does not mean that calculations of the standard theory using a thin-double-layer approximation are incorrect. In other words, except in the region of electrical double layer, the calculation results by the standard theory are correct at least for low voltage problems. Thus, if theoretical evaluations are done for macroscopic characters such as an average flow velocity in a microfluidic channel, we can trust the calculations. Further, the predictions by use of the standard theory are still useful, even for large voltage problems, since the decrease of the flow velocity due to large voltage effects is just about 50% at large voltages (e.g., $v_0 = 40$).

C. Impossibility of exceeding a steric limit in a dilute electrolyte at large voltages

The discrepancy between theoretical and experimental results at large voltages are often discussed from the viewpoint of steric effects or ion crowding effects [3,15,16]. However, at least for a dilute electrolyte ($C_0 < 0.1\ \text{mM}$), it is impossible to exceed a steric limit of ions since the maximum peak concentration in our calculation is just approximately 40 times higher than the initial concentration at $v_0 = 40$, as shown in Fig. 11(a), and the predicted concentration is much smaller than that of water ($40C_0 < 4 \times 10^{-3} \ll 55.6\ \text{M}$). Namely, we find that ions never exceed the steric limit because of the ion-conserving effect for a typical 2D microfluidic geometry ($W_0 = 100\ \mu\text{m}$, $c = 10\ \mu\text{m}$, and $C_0 < 0.1\ \text{mM}$) of ICEO, and, thus, we usually need not consider the ion crowding effect. This is reasonable since ions cannot diffuse so fast; thus, we should

consider a microcanonical ensemble, as mentioned for the 1D geometry in Ref. [20], even for the 2D geometry on ICEO.

D. Steady-state subject to a large applied voltage

We initially doubted that the plateaus in Fig. 7(d) correspond to quasi steady states since there are plenty of ions in a 2D liquid chamber and the charging time is much smaller than the diffusion time T_d . However, surprisingly, we cannot find any tendency to change the states. Thus, we believe that the observed states are really steady states that appear with many subtle balances at large voltages. Further, we find that the ion-shortage region that appears in the steady ICEO flow at large voltages is limited within a few Debye length as described by d_{eff} in our ion-conserving theory and the distribution of ρ in the r direction becomes similarly independent of θ in an electro double layer within the charging time and the distribution keeps in the steady state because of the balance between the in- and out-flows to the concerning region, as shown in Fig. 10(b). We believe that this insight also helps our understandings concerning why the ion concentration never exceeds the steric limit at large applied voltages albeit there are many ions in the 2D region.

E. Decrease of performance in a dense electrolyte (>100 mM)

However, for a dense electrolyte (>100 mM), the situation differs. Namely, for a dense electrolyte ($C_0 > 100$ mM), the maximum peak concentration becomes higher than 4 M at $v_0 = 40$; i.e., the maximum ion concentration becomes comparable to 10% of the concentration of water (55.6 M). Thus, steric effects may appear as predicted by Bazant *et al.* [3]. In fact, the decrease of flow velocity in a dense solution (>10 or 100 mM) is also reported by many researchers [3,8,22,24,25]. For example, Hanett *et al.* [8] reported that for less than 0.1 mM KCl the concentration of the KCl solution had little effect on ICEO velocities; however, as the KCl concentration was increased above this concentration the ICEO velocities decreased, and they ceased at 100 mM KCl. In this sense, the study of steric effects [3,15,16] is still important and we need more systematic research for this problem.

F. Ideal limit on an ICEO flow

Related to the above discussion, in the experiments on ICEO, the large flow velocity comparable to the velocity of the standard theory is always obtained in distilled water or extremely dilute KCl solutions; i.e., an ideal solution of ICEO is water of pH = 7. Thus, to consider the calculation for water of pH = 7 (i.e., $C_0 = 10^{-7}$ M and $\lambda_D = 1$ μm) is important as an ideal limit on an ICEO flow. In particular, for promising biomedical applications such as laboratory-on-a-chip, the calculations for $W_0 = 100$ μm (i.e., $\kappa = W_0/\lambda_D = 100$) are interesting since the typical channel width is on the order of 100 μm . It should be noted that since typical concentrations of ordinary electrolytes are $C_0 = 10^{-5}$ to 10^{-1} M, the Debye length is often referred to in the standard textbooks as $\lambda_D = 1$ to 100 nm; however, the Debye length λ_D ($\equiv \sqrt{\epsilon kT/2z^2 e^2 C_0}$) of $C_0 = 10^{-7}$ M is 1 μm . Further, many experiments on ICEO start from a 0.001 mM KCl solution, except water, since a 0.0001 mM KCl solution cannot neglect the existence of H^+

and OH^- . Of course, by using nondimensional formulations with u_0 , we can forget real values during calculations. e.g., the experiment corresponding to Fig. 8(a) can be done by changing the size of W_0 from 50 to 100 μm for water, instead of changing the concentration at the fixed width (e.g., $W_0 = 10$ μm). In addition, our calculations are consistent with the experimental fact that the observed ICEO velocities are not largely dependent on the concentration in a dilute range (<0.1 mM), although the peak velocity slightly depends on κ , as shown in Fig. 8(a).

G. Stable direct simulation considering flow effects

By using the stable FE-FV method, we perform complete multiphysics calculations on ICEO at large voltages and clarify the details of the finite electro double layer on ICEO. In particular, we find that the decrease of slip velocity at large voltages is successfully explained by the shortage of ions due to the ion-conserving phenomena as shown in Fig. 8(b). Further, we find that the flow in the double layer at large voltages surprisingly affects redistributions of the surface charge density and induces a homogeneous distribution in the double layer independent of θ , as shown in Fig. 10(b). Thus, in the future, we also want to develop an analytical theory to consider this phenomenon.

Further, just recently, Davidson *et al.* have shown direct numerical simulations of the coupled Poisson-Nernst-Planck and Navier-Stokes equations for an electrolyte around a polarizable cylinder subject to an external electric field and found a novel chaotic flow phenomenon around a cylinder at high applied electric fields [26]. This is an excellent calculation as pioneering work; however, in a system of small Reynolds number (Re), the flow becomes a laminar flow and we cannot expect a turbulent flow; thus, the existence of the chaotic flow at small Reynolds number is questionable from the viewpoint of physics. Further, mathematically, it is well known that the origin of the turbulent flow is the inertial term [especially the nonlinear term $(\mathbf{u} \cdot \nabla_n)\mathbf{u}$] in the Navier-Stokes equations [Eq. (14)] and the other linear terms do not cause a turbulent flow; thus, from the viewpoint of mathematics, the existence of the chaotic flow is also questionable since the authors do not use the nonlinear term $(\mathbf{u} \cdot \nabla_n)\mathbf{u}$. Furthermore, from the viewpoint of the numerical calculation method, the existence of a lot of numerical instabilities is well known. Thus, we cannot deny the possibility that numerical instability causes the chaotic flow in their calculations.

Specifically, on the one hand, Davidson *et al.* used second-order finite differences in cylindrical coordinates on a staggered mesh; however, it is not enough to conserve the ion numbers and it may cause numerical instability. Further, although they claimed that they used nondissipative numerical advection, the time evolution using the time differential term may cause a large numerical error because of the large factor of $\Delta t/\text{Re}$; in particular, in our trial, the common time-evolution method that considers the incompressible condition separately through the Poisson equation for pressure, often causes numerical instability since it is a half-implicit method that requires relatively large Reynolds number for stable calculations. On the other hand, as mentioned in Sec. II D and Appendix A, to avoid the numerical instability, we use the

Stokes equation that removes the inertial term completely [i.e., Eq. (20)] and solve two equations [in Eq. (20)] simultaneously by use of the direct FEM for the Stokes equation; then ions are moved according to the Nernst-Planck equation by using the finite-volume method that conserves ion numbers completely. In other words, differing from Davidson *et al.*'s calculations, our calculations are stabilized completely from the viewpoint of the numerical calculation technique, and, moreover, their reliability is examined by the comparison between the analytical results and numerical results. We believe that this is the main reason we do not observe a chaotic flow even at large electric fields.

H. Meaning of ICEO analysis in microfluidic applications

In microfluidic applications such as laboratory-on-a-chip [27], pumps, valves, and mixers are usually fabricated and analyzed for planar structures (structures made by use of a thin-film process). This is because the fabrication of planar structures is easier than that of high-aspect-ratio structures (structures in which the ratio of the height to the width is high). However, because of the development of process technologies such as deep reactive ion etching, the fabrication of high-aspect-ratio structures has also become a realistic option [7]. Thus, analysis of ICEO phenomena that are typically represented by Fig. 1(a) is directly useful to consider such high-aspect-ratio devices using ICEO phenomena [2,7,10,11]. Further, the fundamental understanding of 2D ICEO flows often accelerates the development of planar devices; e.g., high-speed ACEO pumps of the order of 1 mm/s have been developed, as suggested by the ICEO concept [5]. Moreover, we believe that the fundamental understanding of ICEO makes it possible to design microfluidic devices using surface phenomena as we intended. Therefore, we believe that our analysis is important for microfluidic applications.

IX. CONCLUSION

In conclusion, for a small size system ($< \sim 1$ mm) with a low conductivity due to a low concentration ($< \sim 10$ mM), we have clarified dc step response phenomena on ICEO flows around a cylinder between parallel electrodes at small and large applied voltages at the finite thickness of an electrical double layer: (1) By using a multiphysics coupled simulation technique based on the finite-element method and finite-volume method, we observe that quadrapolar ICEO vortex flows grow around a cylinder during the charging time of the cylinder for both unbounded and bounded systems and decay during the charging time of the parallel electrodes only for a bounded system using blocking electrodes on the application of large and small dc voltages; (2) by proposing a simple response model that considers the 2D PNP equations, we successfully elucidate the step response time of ICEO flow at large and small applied voltages; (3) by solving 2D-steady PNP equations around a cylinder, we find the exact solutions on a steady diffusion ion problem at small applied voltages for an unbounded problem and find that the solutions agree well with the results obtained by use of the multiphysics coupled simulation technique; (4) by solving a 2D-steady Stokes equation having an electric stress term around a cylinder,

we find the analytical formulations on an ICEO flow in a finite electrical double layer at small applied voltages for an unbounded problem and find that the solutions agree well with the results obtained by use of the multiphysics coupled simulation technique; (5) by considering an ion-conserving condition along with 2D-steady Stokes-PNP equations, we successfully explain significant decrease of the maximum slip velocity at large applied voltages; (6) by considering flow effects on ion distributions, we find that the motion of liquid affects redistributions of surface charge density and forms a homogeneous surface distribution not depending on θ . We believe that our analysis will be useful for designing prospective microfluidic devices.

APPENDIX A: DETAILS OF THE COUPLED SIMULATION METHOD FOR THE POISSON-NERNST-PLANCK-STOKES EQUATIONS (FE-FV METHOD)

1. FVM for the NP equations on c_{\pm}

The FVM is a numerical method for solving partial differential equations that calculate the values of the conserved variables averaged across the volume and thus preserve the number of ions well, while ordinary numerical methods often do not preserve the number of ions [18]. Please note that although we are not dealing with ion particles but densities of ions, by considering a small control volume V_i with a surface S_i for i -th cell, we can conserve ion number of the system. Namely, by integrating Eq. (12) over the control cell with the Gauss's theorem, we obtain the basic continuity equations (of the FVM) that

$$\frac{\partial}{\partial t} \iiint_{V_i} c_{\pm} dv = - \iiint_{V_i} \nabla \cdot \mathbf{f}_{\pm} dv = - \iint_{S_i} \mathbf{f}_{\pm} ds. \quad (\text{A1})$$

Thus, as shown in Fig. 1(c), by considering an unstructured quadrilateral element having a center point for c_{\pm}^i at the position \mathbf{x}^i of i -th cell, we can discretize Eq. (A1) as follows:

$$V_i \frac{c_{\pm}^{i,n+1} - c_{\pm}^{i,n}}{\Delta t} + \sum_{j=1}^{j=4} \mathbf{f}_{\pm,ij}^{n+1} \cdot \mathbf{n}_{ij} S_{ij} = 0, \quad (\text{A2})$$

where $\mathbf{f}_{\pm,ij}^{n+1}$, $S_{ij} \mathbf{n}_{\pm,ij}$, are the flux, the boundary area, and the outward unit vector normal to S_{ij} , respectively, between i -th and j -th cells; n is a time step number and thus $\mathbf{f}_{\pm,ij}^{n+1}$ shows the flux of the next step. In addition, to perform stable calculations, we develop an implicit method for $c_{\pm,i}$ by assuming that

$$\begin{aligned} \mathbf{f}_{\pm,ij}^{n+1} \cdot \mathbf{n}_{ij} &= \frac{c_{\pm}^{i,n+1} - c_{\pm}^{j,n+1}}{d_{ij}} \mathbf{j}_{ij} \cdot \mathbf{n}_{ij} \\ &\pm c_{\pm,ij}^n \frac{\phi^{i,n} - \phi^{j,n}}{d_{ij}} \mathbf{j}_{ij} \cdot \mathbf{n}_{ij} + c_{\pm,ij}^n \mathbf{u}_{ij}^n \cdot \mathbf{n}_{ij}, \end{aligned} \quad (\text{A3})$$

where \mathbf{u}_{ij}^n is the velocity between the i -th and j -th cells and it is obtained from the calculation of the FEM for the Stokes equations as the midnode value of S_{ij} , $c_{\pm,ij}^n = (c_{\pm}^{i,n} + c_{\pm}^{j,n})/2$, d_{ij} is a distance between the i -th center point and the j -th center point, $\phi^{i,n+1} (= \frac{1}{4} \sum_{\beta=1}^4 \phi_{\beta})$ is a center value of ϕ at i -th cell, and $\mathbf{j}_{ij} = (\mathbf{x}^j - \mathbf{x}^i)/|\mathbf{x}^j - \mathbf{x}^i|$. Thus, by substituting

Eq. (A3) into Eq. (A2), we obtain

$$\begin{aligned} & \left(1 + \sum_j^{j=4} G_{ij}^A\right) c_{\pm}^{i,n+1} - \sum_j^{j=4} G_{ij}^A c_{\pm}^{j,n} \\ &= c_{\pm}^{i,n} \mp \sum_j^{j=4} G_{ij}^A c_{\pm,ij}^n \delta\phi^{ij,n} - \sum_j^{j=4} G_{ij}^B c_{\pm,ij}^n \mathbf{u}_{ij}^n \cdot \mathbf{n}_{ij}, \end{aligned} \quad (\text{A4})$$

where $\delta\phi^{ij,n} = \phi^{i,n} - \phi^{j,n}$, $G_{ij}^A = \frac{\Delta t S_{ij}}{V_i d_{ij}} (\mathbf{j}_{ij} \cdot \mathbf{n}_{ij})$, and $G_{ij}^B = \frac{\Delta t S_{ij}}{V_i}$. It should be noted that since Eq. (A4) provides the linear matrix formulation $A\{c_{\pm}^{i,n+1}\} = \mathbf{b}$, we can obtain $c_{\pm}^{i,n+1}$ implicitly. Further, since $\mathbf{f}_{\pm,ji}^{n+1} \cdot \mathbf{n}_{ji} S_{ji} = -\mathbf{f}_{\pm,ij}^{n+1} \cdot \mathbf{n}_{ij} S_{ij}$, we can observe that the number of ions is conserved in the system during numerical simulations within the accuracy of floating point error by this method.

2. FEM for the Poisson equation on ϕ

Once we obtain $c_{\pm}^{i,n+1}$, we can calculate ϕ from Eqs. (11), (15), and (16) based on the FEM [18,19]. Here, we use a formulation using the Galerkin method. Namely, we first multiply Eq. (11) by a weigh function ($-w_i$) and then integrate the equation over the whole region V ; thus we obtain following equations:

$$\int_V (-w_i) \left[\chi \left(\frac{\partial^2 \phi}{\partial x^2} + \frac{\partial^2 \phi}{\partial y^2} \right) + \rho \right] dV = 0, \quad (i = 1 \text{ to } n_N), \quad (\text{A5})$$

where $\chi = 2\epsilon^2$ and n_N is a total number of the node for ϕ (and \mathbf{u}). By using the Green-Gauss's theorem with a natural boundary condition of Eq. (16), we obtain the following:

$$\sum_{e=1}^{n_e} \int_{V_e} \left[\chi \left(\frac{\partial w_i}{\partial x} \frac{\partial \phi}{\partial x} + \frac{\partial w_i}{\partial y} \frac{\partial \phi}{\partial y} \right) - w_i \rho \right] dV = 0, \quad (i = 1 \text{ to } n_N), \quad (\text{A6})$$

where n_e is a total number of the element and V_e is a region of the e -th element. Here, we can assume ϕ as

$$\phi \simeq \sum_{j=1}^{n_n} M_j \phi_j, \quad (\text{A7})$$

where ϕ_j is a j -th node value of ϕ , $n_n (= 8)$ is a total number of node within a e -th element, and M_j is an interpolation function of j -th element. Thus, by choosing w_i as an interpolation function M_j within the e -th element and as zero in other regions, we obtain

$$\begin{aligned} & \sum_{e=1}^{n_e} \int_{V_e} \chi \left(\frac{\partial M_i}{\partial x} \frac{\partial M_j}{\partial x} + \frac{\partial M_i}{\partial y} \frac{\partial M_j}{\partial y} \right) dV \phi_j \\ &= \sum_{e=1}^{N_e} \int_{V_e} M_i \rho dV, \quad (i = 1 \text{ to } n_N). \end{aligned} \quad (\text{A8})$$

It should be noted that from Eq. (A8) we obtain a global matrix equation $[K]\{\phi\} = \{F\}$ and thus we obtain ϕ_i by using a Dirichlet boundary condition of Eq. (15).

In practice, it is convenient to consider a local matrix equation $[K^e]\{\phi\} = \{F^e\}$, where

$$K_{ij}^e = \chi \int_{V_e} \left(\frac{\partial M_i}{\partial x} \frac{\partial M_j}{\partial x} + \frac{\partial M_i}{\partial y} \frac{\partial M_j}{\partial y} \right) dV, \quad (\text{A9})$$

$$F_i^e = \rho_e \int_{V_e} M_i dV. \quad (\text{A10})$$

Since the geometry of the mesh does not change, we calculate the integral of Eqs. (A9) and (A10) just once, although the element charge $\rho_e = c_+ - c_-$ change in time. Thus, we calculate the integral by using a 5-point Gaussian quadrature rule before the time routine. Of course, by using Eqs. (A9) and (A10), we obtain the global matrix as follows: $[K] = \sum_{e=1}^{n_e} [K^e]$ and $\{F\} = \sum_{e=1}^{n_e} \{F^e\}$.

3. FEM for the Stokes equations

In our trial, the marker and cell method that calculates p_β and \mathbf{u}_β separately did not work well because of low values of Re ; thus, we use the direct FEM that calculates the pressure (p_β) and velocity (\mathbf{u}_β) simultaneously [19]. Thus, by multiplying Eq. (20) by a weigh function ($-M_\alpha$ for the stokes equation and $-N_\alpha$ for the continuum equation) and integrating them over the whole region V , we obtain following equations:

$$\sum_{e=1}^{n_e} \int_{V_e} (-M_\alpha) \left[F_i - \frac{\partial p}{\partial x_i} + \mu \left(\frac{\partial^2 u_i}{\partial x_1^2} + \frac{\partial^2 u_i}{\partial x_2^2} \right) \right] dV = 0, \quad (\alpha = 1 \text{ to } n_N, i = 1, 2), \quad (\text{A11})$$

$$\sum_{e=1}^{n_e} \int_{V_e} (-N_\alpha) \left(\frac{\partial u_1}{\partial x_1} + \frac{\partial u_2}{\partial x_2} \right) dV = 0, \quad (\alpha = 1 \text{ to } n_{N_2}), \quad (\text{A12})$$

where $F_i = -F_0 \rho \nabla_n \phi$ and n_{N_2} is a total number of the node for p . By using the Green-Gauss's theorem with a natural boundary condition of Eq. (16), we obtain the following:

$$\sum_{e=1}^{n_e} \int_{V_e} \left[\mu \left(\frac{\partial N_\alpha}{\partial x_1} \frac{\partial u_i}{\partial x_1} + \frac{\partial N_\alpha}{\partial x_2} \frac{\partial u_i}{\partial x_2} \right) - N_\alpha F_i + N_\alpha \frac{\partial p}{\partial x_i} \right] dV = 0, \quad (\alpha = 1 \text{ to } n_N, i = 1, 2), \quad (\text{A13})$$

$$\sum_{e=1}^{n_e} \int_{V_e} \left(u_1 \frac{\partial N_\alpha}{\partial x_1} + u_2 \frac{\partial N_\alpha}{\partial x_2} \right) dV = 0, \quad (\alpha = 1 \text{ to } n_{N_2}). \quad (\text{A14})$$

Thus, similarly to the FEM for ϕ , by assuming

$$\mathbf{u} \simeq \left(\sum_{\beta=1}^8 M_\beta u_{1,\beta}, \sum_{\beta=1}^8 M_\beta u_{2,\beta} \right), \quad p \simeq \sum_{\beta=1}^4 N_\beta p_\beta, \quad (\text{A15})$$

we obtain following local matrix equations:

$$G_{i\alpha}^e \equiv \sum_{\beta=1}^8 K_{\alpha\beta} u_{i\beta}^e + \sum_{\beta=1}^4 H_{\alpha\beta}^i p_\beta^e - F_\alpha^i \quad (\alpha = 1 \text{ to } 8, i = 1, 2), \quad (\text{A16})$$

$$Q_\alpha^e \equiv \sum_{\beta=1}^8 (H_{\beta\alpha}^1 u_{1\beta}^e + H_{\beta\alpha}^2 u_{2\beta}^e) \quad (\alpha = 1 \text{ to } 4), \quad (\text{A17})$$

where

$$K_{\alpha\beta} = \int_{V_e} \mu \left(\frac{\partial M_\alpha}{\partial x_1} \frac{\partial M_\beta}{\partial x_1} + \frac{\partial M_\alpha}{\partial x_2} \frac{\partial M_\beta}{\partial x_2} \right) dV, \quad (\text{A18})$$

$$H_{\alpha\beta}^i = \int_{V_e} M_\alpha \frac{\partial N_\beta}{\partial x_i} dV, \quad (\text{A19})$$

$$F_\alpha^i = \int_{V_e} F_i M_\alpha dV. \quad (\text{A20})$$

Thus, by considering $\sum_e^{n_e} G_{i\alpha}^e = 0$ and $\sum_e^{n_e} Q_\alpha^e = 0$, we obtain a global matrix equations and corresponding solutions; i.e., the node values of \mathbf{u} and p (\mathbf{u}_i and p_i).

APPENDIX B: VARIOUS APPROXIMATIONS FOR AN ICEO FLOW PROBLEM AT SMALL VOLTAGES (MODEL A TO C)

1. Other formulations of the Stokes equation

It is useful to introduce other formulations of the Stokes equation to obtain simple analytical formulations through various approximations. Namely, by using the relation $\nabla_n^2 \mathbf{u}_{\text{eq}} \equiv \nabla_n (\nabla_n \cdot \mathbf{u}_{\text{eq}}) - \nabla_n \times \nabla_n \times \mathbf{u}_{\text{eq}} = -\nabla_n \times \nabla_n \times \mathbf{u}_{\text{eq}}$, we transform Eq. (67) into

$$-\nabla_n \times \nabla_n \times \mathbf{u}_{\text{eq}} = \nabla_n p - F_0 \rho \mathbf{E}, \quad (\text{B1})$$

where $\mathbf{A} \equiv \nabla_n \times \mathbf{u}_{\text{eq}} = A_z \hat{z}$ and

$$A_z = \frac{1}{r} \left[\frac{\partial}{\partial r} (r u_\theta^{\text{eq}}) - \frac{\partial u_r^{\text{eq}}}{\partial \theta} \right]. \quad (\text{B2})$$

Thus, since $\nabla_n \times \mathbf{A} = \frac{1}{r} \frac{\partial A_z}{\partial \theta} \hat{r} - \frac{\partial A_z}{\partial r} \hat{\theta}$, we obtain

$$\frac{\partial}{\partial r} \left[\frac{1}{r} \frac{\partial}{\partial r} (r u_\theta^{\text{eq}}) - \frac{1}{r} \frac{\partial u_r^{\text{eq}}}{\partial \theta} \right] = \frac{1}{r} \frac{\partial p}{\partial \theta} - F_0 \rho E_\theta \quad (\theta \text{ component}), \quad (\text{B3})$$

$$\begin{aligned} & -\frac{1}{r} \frac{\partial}{\partial \theta} \left[\frac{1}{r} \frac{\partial}{\partial r} (r u_\theta^{\text{eq}}) - \frac{1}{r} \frac{\partial u_r^{\text{eq}}}{\partial \theta} \right] \\ & = \frac{\partial p}{\partial r} - F_0 \rho E_r \quad (r \text{ component}), \end{aligned} \quad (\text{B4})$$

with the boundary conditions that

$$\frac{\partial u_\theta^{\text{eq}}}{\partial r} = u_\theta^{\text{eq}} = 0 \quad (\text{at } r = \infty), \quad (\text{B5})$$

$$u_\theta^{\text{eq}} + u_\theta^f = 0, \quad u_r^{\text{eq}} + u_r^f = 0 \quad (\text{at } r = c). \quad (\text{B6})$$

2. Model A (thin-double-layer approximation in the new framework)

If the electrical double layer is very thin, we can approximate Eq. (B3) into

$$\frac{\partial^2}{\partial r^2} (u_\theta^{\text{eq}}) \simeq -F_0 \rho E_\theta \simeq +2F_0 \epsilon^2 \frac{\partial^2 \phi_{\text{eq}}}{\partial r^2} \bar{E}_\theta, \quad (\text{B7})$$

where $\bar{E}_\theta = 2E_0 \sin \theta$. Thus, by integrating Eq. (B7) over r with the boundary conditions [Eqs. (26) and (27)], we obtain

$$u_\theta^{\text{eq}} \simeq +2F_0 \epsilon^2 \phi_{\text{eq}}(r, \theta) \bar{E}_\theta. \quad (\text{B8})$$

Thus, by substituting Eq. (54) into Eq. (B8), we obtain

$$\begin{aligned} u_\theta^{\text{eq}} & \simeq -2F_0 \epsilon^2 \left[\frac{2E_0 c}{K_1(\kappa c)} \right] K_1(\kappa r) \bar{E}_\theta \cos \theta \\ & = -2u_0 \frac{K_1(\kappa r)}{K_1(\kappa c)} \sin 2\theta. \end{aligned} \quad (\text{B9})$$

From Eqs. (64), (73), and (B9), we obtain

$$C_2 = c^3 u_0 \sin 2\theta. \quad (\text{B10})$$

Therefore, from Eqs. (63), (73), and (B9), we obtain

$$u_\theta^{\text{Model A}} \simeq 2u_0 \left[\frac{c^3}{r^3} - \frac{K_1(\kappa r)}{K_1(\kappa c)} \right] \sin 2\theta. \quad (\text{B11})$$

Model A is reasonable and agrees well with the classical concept; however, it remains controversial why we can approximate that $E_\theta \simeq \bar{E}_\theta = 2E_0 \sin \theta$ in spite of the existence of the large changes of E_θ in the electrical double layer.

3. Model B [finite-double-layer approximation considering $E_\theta(r, \theta)$]

In Model B, we consider the distribution of $E_\theta(r, \theta)$ in Eq. (B7). Namely, by integrating Eq. (B7) with the boundary conditions [Eqs. (26) and (27)], we obtain

$$u_\theta^{\text{eq}} \simeq - \int_r^\infty \int_{r''}^\infty F_0 \rho(r', \theta) E_\theta(r', \theta) dr' dr''. \quad (\text{B12})$$

By substituting Eq. (59) into Eq. (B12), we obtain

$$\begin{aligned} u_\theta^{\text{eq}} & \simeq -F_0 \int_r^\infty \int_{r''}^\infty \left[p_1 E_0 \left(1 + \frac{c^2}{r'^2} \right) K_1(\kappa r') - p_1^2 \frac{K_1(\kappa r')^2}{r'} \right] \\ & \quad \times dr' dr'' \sin 2\theta. \end{aligned} \quad (\text{B13})$$

Here, by using characteristics of Bessel function, we obtain

$$K_n(\kappa r) \simeq \sqrt{\frac{\pi}{2\kappa r}} e^{-\kappa r} \quad (\kappa r > n), \quad (\text{B14})$$

$$\int_r^\infty \frac{K_1(\kappa r')^2}{r'} dr' = -[K_0(\kappa r)^2 - K_1(\kappa r)^2] \simeq 0, \quad (\text{B15})$$

$$\int_r^\infty K_1(\kappa r') dr' = \frac{1}{\kappa} K_0(\kappa r), \quad (\text{B16})$$

$$\begin{aligned} \int_r^\infty \frac{K_1(\kappa r')}{r'^2} dr' & \simeq \int_r^\infty \frac{K_3(\kappa r')}{r'^2} dr' \\ & = -\frac{1}{\kappa r^2} K_2(\kappa r), \end{aligned} \quad (\text{B17})$$

$$\begin{aligned} \int_r^\infty \left(1 + \frac{c^2}{r'^2} \right) K_1(\kappa r') dr' & \simeq \frac{1}{\kappa} K_0(\kappa r) - \frac{c^2}{\kappa r^2} K_2(\kappa r) \\ & \simeq \frac{1}{\kappa} \left(1 - \frac{c^2}{r^2} \right) K_1(\kappa r), \end{aligned} \quad (\text{B18})$$

where we assume $\kappa r > 3$. Thus, under the condition that $\kappa r > 3$, we obtain

$$\int_r^\infty F_0 \rho E_\theta dr' \simeq \frac{F_0 p_1 E_0}{\kappa} \left(1 - \frac{c^2}{r^2} \right) K_1(\kappa r) \sin 2\theta. \quad (\text{B19})$$

Further, by using Eqs. (B14) to (B18) again, we obtain

$$\begin{aligned} u_{\theta}^{\text{eq}} &\simeq - \int_r^{\infty} \int_{r'}^{\infty} F_0 \rho E_{\theta} dr' dr'' \\ &\simeq - \frac{F_0 p_1 E_0}{\kappa^2} \left(1 + \frac{c^2}{r^2}\right) K_1(\kappa r) \sin 2\theta \\ &= -u_0 \left(1 + \frac{c^2}{r^2}\right) \frac{K_1(\kappa r)}{K_1(\kappa c)} \sin 2\theta. \end{aligned} \quad (\text{B20})$$

Therefore, from Eqs. (64), (73), and (B20), we obtain

$$u_{\theta}^{\text{Model B}} \simeq 2u_0 \left[\frac{c^3}{r^3} - \left(1 + \frac{c^2}{r^2}\right) \frac{K_1(\kappa r)}{2K_1(\kappa c)} \right] \sin 2\theta. \quad (\text{B21})$$

4. Model C (finite-double-layer approximation assuming $\frac{\partial}{\partial \theta} = 0$)

In Model C, we just assume $\frac{\partial}{\partial \theta} = 0$ in Eq. (B3) and consider the equation

$$\frac{\partial}{\partial r} \left[\frac{1}{r} \frac{\partial}{\partial r} (r u_{\theta}^{\text{eq}}) \right] \simeq -F_0 \rho E_{\theta}. \quad (\text{B22})$$

Thus, by integrating Eq. (B22) over r with the boundary conditions, we obtain

$$-\frac{1}{r} \frac{\partial}{\partial r} (r u_{\theta}^{\text{eq}}) \simeq -\frac{F_0 p_1 E_0}{\kappa} \left(1 - \frac{c^2}{r^2}\right) K_1(\kappa r) \sin 2\theta. \quad (\text{B23})$$

Here, by using characteristics of Bessel function again, we obtain

$$\int_r^{\infty} r K_1(\kappa r') dr' \simeq \int_r^{\infty} r K_1(\kappa r') dr' \simeq \frac{r}{\kappa} K_0(\kappa r), \quad (\text{B24})$$

$$\int_r^{\infty} \frac{K_1(\kappa r')}{r'} dr' \simeq \int_r^{\infty} \frac{K_2(\kappa r')}{r'} dr' = -\frac{1}{\kappa r} K_1(\kappa r), \quad (\text{B25})$$

$$\begin{aligned} \int_r^{\infty} \left(r' - \frac{c^2}{r'}\right) K_1(\kappa r') dr' &\simeq \frac{r}{\kappa} K_0(\kappa r) + \frac{c^2}{\kappa r} K_1(\kappa r) \\ &\simeq \frac{r}{\kappa} \left(1 + \frac{c^2}{r^2}\right) K_1(\kappa r). \end{aligned} \quad (\text{B26})$$

Thus, by integrating Eq. (B23) with the boundary conditions we obtain

$$r u_{\theta}^{\text{eq}} \simeq -r \frac{F_0 p_1 E_0}{\kappa^2} \left(1 + \frac{c^2}{r^2}\right) K_1(\kappa r) \sin 2\theta. \quad (\text{B27})$$

Thus, we obtain

$$u_{\theta}^{\text{eq, Model C}} = u_{\theta}^{\text{eq, Model B}}, \quad (\text{B28})$$

$$u_{\theta}^{\text{Model C}} = u_{\theta}^{\text{Model B}}. \quad (\text{B29})$$

APPENDIX C: DISCUSSION ON THE DC PROBLEM ON ICEO

1. Meaning of a dc analysis on ICEO as a basis of ac analysis

Practically, ICEO devices are expected to be used under ac electric fields to avoid dc problems such as chemical reactions at the electrodes [2]. Nevertheless, a dc analysis is important to consider fundamental characteristics of ICEO and to consider the practical performance of ICEO devices

under ac electric fields. Actually, a lot of fundamental and applied analyses on ICEO have been done substantially for the steady (or dc) problems as a basis of ac analysis for bounded problems [2,10,11,13]. This is because, once we know the dc charging time for a cylinder and electrodes (e.g., τ_A and τ_B ; $\tau_A < \tau_B$) and the steady slip velocity for the dc step response (e.g., $U_0^{\text{dc}} = \varepsilon c_d E^2 / \mu$), we can approximately predict the average slip velocity on ICEO in the presence of an ac electric field $E^{\text{ac}} = E \cos 2\pi f t$ as $\langle U_0^{\text{ac}} \rangle = \langle \varepsilon c_d E^2 \cos^2 2\pi f t / \mu \rangle = \frac{1}{2} U_0^{\text{dc}}$ in the range of the appropriate frequency (i.e., $\frac{1}{\tau_B} < f < \frac{1}{\tau_A}$) [2,11,13], although many discrepancies between theory and experimental results remain, as discussed in this paper and in Ref. [3,24]. Thus, what we should clarify first is a dc step-response problem even if we are mainly interested in ac problems; however, to clarify a dc step-response problem numerically, we need to use a kind of periodic boundary condition for ion transportation as a numerical calculation technique to consider an unbounded problem in the finite calculation region; thus, we probably also need to discuss nonblocking electrodes along with our intended meanings to clarify our problem, although complex nonblocking electrode problems are beyond the scope of this paper.

2. Ion passing condition for an ac capacitive current

As reviewed in Ref. [17], an electrolyte cell sandwiched by the parallel blocking electrodes is often modeled as a resistor-capacitor (RC) circuit, where R is the resistance due to ion transportation and C is the capacitance due to the electrical double layer on the blocking electrode. Since the capacitor works as ion storage, ions seem to be passing freely through the plane at the outside edge of the electrical double layer in an appropriate frequency. This is a basis of the common treatment that converts ac problems into dc problems on an ICEO analysis. Thus, for the real ac problems, the treatment of the ion flux at the electrode [described in Eq. (9)] or the complete passing condition at the electrode is just a simple model on a charging current that flows into a thin electrical double layer on the electrode (Γ_t or Γ_b); thus, rigorously, the real electrode surfaces should be assumed at $X = 0 - \delta$ and $W_0 + \delta$, where δ is the thickness of the electrical double layer at the top and bottom electrodes. This is the intended physical meaning of the ion passing condition at the electrode [Eq. (9)] and it is the original reason to consider the unbounded problem in this field.

3. Faradaic reaction at the far positions

In experiments, the ICEO can be observed in the dc field. Thus, from the viewpoint of fundamental physics, real dc problems are also important. For instance, we consider water of pH = 7 as an ideal electrolyte (as discussed in Sec. VIII F) and set the platinum (Pt) electrodes at the far positions from the cylinder (e.g., $W'_0 = 2$ mm); in this case, by applying a large voltage (e.g., $V_0 = 20$), we can expect Faradaic reactions at the electrodes [28], i.e., at the anode we can expect the oxidation reaction that $2\text{H}_2\text{O} \rightarrow \text{O}_2 + 4\text{H}^+ + 4e^-$ and at the cathode we can expect the reduction reaction that $4\text{H}_2\text{O} + 4e^- \rightarrow 2\text{H}_2 + 4\text{OH}^-$.

However, it is well known that if we cannot remove the generated ions due to the electrolysis of water (H^+ and OH^- at the anode and cathode, respectively), the above reactions halt automatically; fortunately, at the arrival of the counter ions (OH^- and H^+) by the ion electrophoresis to the electrodes, the unwanted generated ions are removed promptly by the reaction $OH^- + H^+ \rightarrow H_2O$, and, at the same time, the excess surface ions transported from the bulk region are expelled promptly. Please note that by this process, total numbers of ions (OH^- and H^+) may decrease; however, since we consider a long electrode distance (W_0), they are supplied in the wide bulk region by the reaction $H_2O \rightarrow OH^- + H^+$; thus, we can assume that the numbers of ions (H^+ and OH^-) are constant in the bulk region and the ions pass freely at $X = 0$ and W_0 (e.g., $W_0 = 100 \mu\text{m}$), as we assumed in our numerical method.

Furthermore, since we can assume large resistance of the bulk region for water of $\text{pH} = 7$, the above process is considered to be a diffusion-limited process although the steady dc electric field is kept by the Faradaic reaction at the electrodes. In other words, most of the applied voltage is used in the bulk region, although the thermodynamic potential ($V'_{\text{eq}} = 1.23 \text{ V}$) and the small overpotential (V_η) are required; i.e., the bulk potential difference $V_R = V'_0 - V'_{\text{eq}} - V'_\eta \simeq V'_0$ since $V_R \gg (V'_{\text{eq}} + V_\eta)$ under the far electrode condition. Therefore, by using the electrodes at the far position and applying a large voltage, we can perform the dc step-response experiment corresponding to our dc unbounded problems that are analyzed analytically and numerically in our theory; in particular, the ion passing condition in Eq. (9) is justified as a substitute numerical model for a dc Faradaic reaction at the far positions under the condition that $E = V_0/W_0 = (V'_0 - V'_{\text{eq}} - V'_\eta)/W'_0 \simeq V'_0/W'_0$. Please note that the concentrations of ions are assumed to be symmetrical to the plane at $X = 0$ since the amount of the consumed anion at the anode is same as that of the consumed cation at the anode during the Faradaic reactions.

4. Frumkin-Butler-Volmer equation

At the so-called nonblocking electrode that passes a Faradaic current due to a chemical reaction, there are various chemical reactions that depend on the material of electrodes and ion species; e.g., electrolysis of water, deposition of metal, formation of oxidized film, and so on. Thus, if we consider the nonblocking electrode that passes a Faradaic current, we need to clarify the physical meaning and model the electrochemical electrode reactions. In the above part, we clarified the physical meaning for the electrode at the far position in water of $\text{pH} = 7$ and we believe that the justification is enough for our problem.

However, a more sophisticated treatment of the nonblocking electrode might be required for the small gap electrodes (e.g., $W_0 \leq 100 \mu\text{m}$) and it is known as the generalized Frumkin-Butler-Volmer (gFBV) equation [29–32], although the specific treatment based on the gFVB equation for the electrolysis of water is not well known, unfortunately, to the best of my knowledge [28]. Thus, as a first attempt, we start from a common system that consists of a CuSO_4 water solution at the concentration of C_0 with parallel Cu electrodes, as shown in Fig. 1(a). In this case, the main oxidation reaction at the anode is $\text{Cu(s)} \rightarrow \text{Cu}^z + (\text{aq}) + ze^-$, while the main reduction

reaction at the cathode is $\text{Cu}^{z+} + ze^- \rightarrow \text{Cu(s)}$, where $z = 2$ and the suffixes (s) and (aq) represent the solid and aqua states, respectively. Thus, we can assume that the total number of the reactive anion (Cu^{2+}) is constant through the Faradaic reactions, while the total number of the inert anion (SO_4^{2-}) is also constant.

Consequently, by considering the gFBV equation [29–32], we can write the dimensional fluxes at the electrodes as

$$\mathbf{F}_-^{X=0, W_0} = 0, \quad (\text{C1})$$

$$\mathbf{F}_+^{X=0} = - \left[K_R C_O^{\text{Cu}^{2+}} \exp \left(-\alpha_R \frac{ze}{kT} \Delta \Phi_s \right) - K_O C_R^{\text{Cu}} \exp \left(+\alpha_O \frac{ze}{kT} \Delta \Phi_s \right) \right] \mathbf{i}, \quad (\text{C2})$$

$$\mathbf{F}_+^{X=W_0} = + \left[K_R C_O^{\text{Cu}^{2+}} \exp \left(-\alpha_R \frac{ze}{kT} \Delta \Phi_s \right) - K_O C_R^{\text{Cu}} \exp \left(+\alpha_O \frac{ze}{kT} \Delta \Phi_s \right) \right] \mathbf{i}, \quad (\text{C3})$$

where $\Delta \Phi_s$ is the potential drop across the Stern layer, $\alpha_O (= \alpha)$ and $\alpha_R (= 1 - \alpha)$ are the transfer coefficients (e.g., $\alpha_R = \alpha_O = 0.5$), $C_O^{\text{Cu}^{2+}} (= C_+)$ and C_R^{Cu} are concentrations of the reacting species in the oxidized and reduced state at the reaction plane equated with the Stern layer, and K_O and K_R are kinetic rate constants for the oxidation and reduction reactions, respectively. Here we can assume that $K_O C_R^{\text{Cu}} = J_0$ is constant and the concentrations of H^+ and OH^- are negligible.

Of course, we can write the corresponding nondimensional fluxes at the electrodes as

$$\mathbf{f}_-^{x=0,1} = 0, \quad (\text{C4})$$

$$\mathbf{f}_+^{x=0} = -[k_R c_+ \exp(-\alpha_R \Delta \phi_s) - j_0 \exp(+\alpha_O \Delta \phi_s)] \mathbf{i}, \quad (\text{C5})$$

$$\mathbf{f}_+^{x=1} = +[k_R c_+ \exp(-\alpha_R \Delta \phi_s) - j_0 \exp(+\alpha_O \Delta \phi_s)] \mathbf{i}, \quad (\text{C6})$$

where $k_R = K_R/K_c$, $k_O = K_O/K_c$, $j_0 = J_0/(K_c C_0)$, and $\Delta \phi_s = \Delta \Phi_s / (kT/ze)$. According to custom, here we consider the ordinary Boltzmann equation and obtain $c_+ = c_0 \exp(-\phi_D)$, where $c_0 = 1$, $\phi_D (= \phi_{rp} - \phi'_i)$ is the potential drop across the double layer, ϕ_{rp} is a potential of a reaction plane (i.e., the interface between the diffused and Stern layers), and ϕ'_i is the potential of the outer edge of the electrical double layer. Further, we define

$$\Delta \phi \equiv \Delta \phi_s + \Delta \phi_s, \quad (\text{C7})$$

which is the potential difference across the full interface that consists of the Stern and diffused layers. Therefore, from the zero flux condition ($\mathbf{f}_+ = 0$) we obtain the equilibrium potential difference across the interface as

$$\Delta \phi^{\text{eq}} = \ln(k_R c_0 / j_0). \quad (\text{C8})$$

Thus, by defining the over potential as

$$\eta \equiv \Delta \phi - \Delta \phi^{\text{eq}}, \quad (\text{C9})$$

we obtain

$$f_+^{x=0} = -j_0 \exp(+\alpha \Delta \phi_s^{x=0}) [\exp(-\eta^{x=0}) - 1] i, \quad (\text{C10})$$

$$f_+^{x=1} = +j_0 \exp(+\alpha \Delta \phi_s^{x=1}) [\exp(-\eta^{x=1}) - 1] i, \quad (\text{C11})$$

as pointed out in Ref. [29]; obviously, these equations clarify the concept of the overpotential and the physical meaning of a Faradaic current in our problem; e.g., for the steady $\text{CuSO}_4(\text{aq})/\text{Cu}(\text{s})$ system, $\eta^{x=1}$ becomes negative at $x = 1$, while $\eta^{x=0}$ becomes positive at $x = 0$; thus, we obtain $f_+^{x=0} = f_+^{x=1} > 0$. It should be noted that in the next part we use a model that differs a little from Ref. [29] to clarify the asymmetrical Faradaic problem at the Gouy-Chapman (GC) limit.

5. Electrode potential due to a residual charge

It seems that by using Eqs. (C2) and (C3) we can numerically calculate the time evolution of $C_+^{\text{Cu}}(X, Y)$, $C_-^{\text{SO}_4^{2-}}(X, Y)$, a flow field, etc., by setting J_0 and K_R with the condition that $\Delta \Phi_s = 0$ [i.e., no Stern layer condition or the GC limit]. However, since $F_+^{x=0}$ and $F_+^{x=W_0}$ can differ from each other in the gFBV scheme, we need to consider the electrode potential (Φ_1 and Φ_2 at $X = 0$ and W_0 , respectively) of a residual charge (Q_1 and Q_2) due to a Faradaic reactions. Namely, instead of Eq. (5), we can consider that

$$\begin{aligned} \Phi &= +0.5V_0 + \Phi_1 \text{ on } \Gamma_t, \quad \Phi = -0.5V_0 \text{ on } +\Phi_2\Gamma_b, \\ \Phi &= (\Phi_1 + \Phi_2)/2 \text{ on } \Gamma_m, \end{aligned} \quad (\text{C12})$$

where

$$\Phi_1 = \frac{\lambda_D}{\varepsilon} Q_1, \quad \Phi_2 = \frac{\lambda_D}{\varepsilon} Q_2. \quad (\text{C13})$$

Please note that for a small voltage theory that is consistent with the customary assumption [$C_+ \simeq C_0 \exp(-\Phi_D)$] the double layer capacitance per unit area is represented by $C_D \simeq \varepsilon/\lambda_D$; thus, the double layer charge per unit area is represented by $Q \simeq \Phi_D \varepsilon/\lambda_D$; thus, Eq. (C13) is justified as the electrode potential due to the residual charge. Further, physically, when we consider a single metal electrode, the electrode potential becomes negative as the metal dissolves in solution as a positive ion and the electron remains at the electrode, and the process goes to equilibrium under the condition that $K_R C_0 \exp(-\Phi_D) = J_0$; therefore, the equilibrium electrode potential is equivalent with the equilibrium double-layer potential (i.e., $\Phi_D^{\text{eq}} = \ln K_R C_0/J_0$) and it is a reasonable as a physical model. Moreover, when we consider a two-electrode system [e.g., $(+)\text{Zn}|\text{CuSO}_4(\text{aq})|\text{Cu}(-)$] and connect electrically between the electrodes with an external resistance R_{ex} , we can observe a galvanic potential difference $\Phi_2^{\text{Cu}} - \Phi_1^{\text{Zn}}$ and observe an external current $(\Phi_2^{\text{Cu}} - \Phi_1^{\text{Zn}})/R_{\text{ex}}$; thus, Eq. (C13) is reasonable as a general physical model. In addition, a two-electrode system of the same metal (e.g., Cu), by considering an inside resistance R_i of a power source with the applied voltage V_0 , we can assume an external adjustment current $I_{21} = (\Phi_2 - \Phi_1)/R_i$ and the time evolution of Q_1 and Q_2 is described by the following differential

equations:

$$S \frac{dQ_1}{dt} = -\frac{\Phi_2 - \Phi_1}{R_i} - ezS F_+^{x=0}, \quad (\text{C14})$$

$$S \frac{dQ_2}{dt} = +\frac{\Phi_2 - \Phi_1}{R_i} + ezS F_+^{x=1}, \quad (\text{C15})$$

where S is an area of the electrode. It should be noted that our model is useful for the GC limit, and we can numerically calculate the complex time evolution problem by using Eqs. (C1) to (C3) with Eqs. (C12) to (C15), although the detail analysis of the complex behavior due to an asymmetrical behavior of the positive and negative ions is beyond the scope of this paper. Further, our discussion clarifies that the behavior of the two-electrode system $[(+)\text{Zn}|\text{CuSO}_4(\text{aq})|\text{Cu}(-)]$ intrinsically differs from the model described in Sec. II in the sense that it is asymmetrical; nevertheless, in the limit of $W_0 \rightarrow \infty$, the dimensional charging time $\tau_B T_0 = W_0 \lambda_D/D$ becomes infinite. Thus, the response equation for the bounded problem [Eq. (175)] becomes equivalent with the response equation for the unbounded problem [Eq. (174)] for any system. Namely, in the limit of $W_0 \rightarrow \infty$, we can experimentally expect a dc step response described by Eq. (174) during the interested time scale for any system.

APPENDIX D: RELATION BETWEEN THE NERNST-PLANCK EQUATIONS AND “THE BOLTZMANN EQUATION”

1. The Nernst-Planck equation for a steady state

For the steady problem, the NP equations [Eqs. (11) and (12)] are simplified into

$$\nabla_n \cdot (\nabla_n c_{\pm} \pm c_{\pm} \nabla_n \phi - c_{\pm} \mathbf{u}) = 0. \quad (\text{D1})$$

Equation (D1) shows an ion-conserving condition that considers both an inflow and an outflow in a closed region. Since we assume that the total potential ϕ consists of the equilibrium potential ϕ_{eq} and the external potential ϕ_f , by substituting Eq. (22) ($\phi \equiv \phi_{\text{eq}} + \phi_f$) into Eq. (D1), we obtain

$$\nabla_n \cdot [\nabla_n c_{\pm} \pm c_{\pm} \nabla_n \phi_{\text{eq}} \pm c_{\pm} \nabla_n \phi_f - c_{\pm} \mathbf{u}] = 0, \quad (\text{D2})$$

where the second and third terms describe the ion flux due to the equilibrium electric field and external electric field, respectively, and the fourth term describes ion flux due to the macroscopic flow.

2. “The Boltzmann equation” for a steady state

If we assume that

$$c_{\pm} = c_q e^{\mp \phi_{\text{eq}}}, \quad (\text{D3})$$

we obtain that

$$\nabla_n c_{\pm} \pm c_{\pm} \nabla_n \phi_{\text{eq}} = 0, \quad (\text{D4})$$

because

$$\nabla_n c_{\pm} = \nabla_n [c_q e^{\mp \phi_{\text{eq}}}] = \left[\frac{\partial}{\partial \phi_{\text{eq}}} c_q e^{\mp \phi_{\text{eq}}} \right] \nabla_n \phi_{\text{eq}} = \mp c_{\pm} \nabla_n \phi_{\text{eq}}, \quad (\text{D5})$$

where c_q is a general nondimensional bulk concentration and it should be determined from the ion-conserving condition [20,21]. In other words, Eq. (D3) is equivalent with Eq. (D4) under the condition that the numbers of ions are conserved (i.e., ion-conserving condition). Usually, Eq. (D3) is called “the Boltzmann equation” and it is physically justified for a small voltage problem ($|\phi| < 1$) in an equilibrium state. However, if we use it instead of Eq. (D4), there is no limitation of voltage since it is just mathematical transformation. In particular, for the one-dimensional (1D) system which total potential can be described only by the equilibrium potential (i.e., $\phi_f = 0$) and in which \mathbf{u} is obviously zero, we can use Eq. (D3) instead of the Nernst-Planck equations for the steady state even for a large voltage problem, as shown in the ion-conserving Poisson-Boltzmann theory [20].

3. Formal requirement to replace the NP equations with “the Boltzmann equation”

By substituting Eq. (D4) into Eq. (D2), we obtain that

$$\nabla_n \cdot [\pm c_{\pm} \nabla_n \phi_f - c_{\pm} \mathbf{u}] = 0. \quad (\text{D6})$$

This is the formal requirement to replace the NP equations with “the Boltzmann equation.” Further, by considering Eq. (24) ($\nabla_n^2 \phi_f = 0$) and the second equation of Eq. (20) ($\nabla_n \cdot \mathbf{u} = 0$), it is transformed into

$$\nabla_n c_{\pm} \cdot (\nabla_n \phi_f \mp \mathbf{u}) = 0. \quad (\text{D7})$$

Furthermore, by substituting Eq. (D5) into Eq. (D7) with $c_{\pm} \neq 0$, we obtain that

$$\nabla_n \phi_{\text{eq}} \cdot (\nabla_n \phi_f \mp \mathbf{u}) = 0. \quad (\text{D8})$$

4. Approximation of the NP equation for the outside problem ($r \geq c + \epsilon$)

For the outside region of the electrical double layer on the cylindrical metal ($r \geq c + \epsilon$) we can assume $\nabla_n c_{\pm} \simeq 0$ physically although mathematically we need to check the

self-consistency from the results [Eq. (54) and Eq. (115)]. Thus, the requirement of Eq. (D7) is satisfied in a self-consistent manner by the assumption of Eq. (D3). Therefore, we can approximate Eq. (D2) as

$$\nabla_n \cdot [\nabla_n c_{\pm} \pm c_{\pm} \nabla_n \phi_{\text{eq}}] \simeq 0 \quad (\text{for } r \geq c + \epsilon) \quad (\text{D9})$$

for any applied voltage. Namely, for the outside region ($r \geq c + \epsilon$) at any voltage, the steady NP equation [Eq. (D1)] is represented by “the Boltzmann equation” [Eq. (D3)] under the condition that the numbers of ions are conserved.

5. Approximation of the NP equation for the inside problem ($c \leq r < c + \epsilon$)

For the inside region of the electrical double layer ($c \leq r < c + \epsilon$), physically we can assume that $\nabla_n \phi_{\text{eq}} \neq 0$ and $\nabla_n \phi_f \mp \mathbf{u} \neq 0$ because of the existence of the diffused ions; and, specifically, $\nabla_n \phi_f \mp \mathbf{u}$ is approximately parallel to the surface of the circular cylinder and $\nabla_n \phi_{\text{eq}}$ is approximately perpendicular to the surface. Thus, physically, the two vectors [$\nabla_n \phi_{\text{eq}}$ and $\nabla_n \phi_f \mp \mathbf{u}$] cross approximately at right angles and Eq. (D8) is satisfied, although mathematically we also need to check the self-consistency from the results [Eq. (54) and Eq. (115)]. It should be noted that, physically, $\nabla_n \phi_f$ results from the electrostatic shield due to the diffused ions and \mathbf{u} results from $\nabla_n \phi_f$; further, $\nabla_n \phi_{\text{eq}}$ mainly represents the fade-out of the initial electric field perpendicular to the surface. We can expect that the strength of the equilibrium electric field is much stronger than that of the external field except $r \simeq c + \epsilon$ because of the large charge in the diffused ion layer; thus, we can assume that $|\nabla \phi_{\text{eq}}| \gg |\nabla \phi_f|$ for $c \leq r < c + \epsilon$, i.e., we can neglect the flux due to the external field for $c \leq r < c + \epsilon$. It should be noted that the results [Eq. (54) and Eq. (115)] obtained by replacing the NP equation with the Boltzmann equation obviously satisfy the ordinary physical conditions [Eq. (D7) or Eq. (D8)]; thus, the replacement is justified.

-
- [1] N. I. Gamayunov, V. A. Murtsovkin, and A. S. Dukhin, *Colloid J. USSR* **48**, 197 (1986).
- [2] M. Z. Bazant and T. M. Squires, *Phys. Rev. Lett.* **92**, 066101 (2004).
- [3] M. Z. Bazant, M. S. Kilic, B. D. Storey, and A. Ajdari, *Adv. Colloid Interf. Sci.* **152**, 48 (2009).
- [4] A. Ramos, H. Morgan, N. G. Green, and A. Castellanos, *J. Colloid Interf. Sci.* **217**, 420 (1999).
- [5] J. P. Urbanski, T. Thorsen, J. A. Levian, and M. Z. Bazant, *Appl. Phys. Lett.* **89**, 143508 (2006).
- [6] C.-C. Huang, M. Z. Bazant, and T. Thorsen, *Lab Chip* **10**, 80 (2010).
- [7] H. Sugioka, *Phys. Rev. E* **78**, 057301 (2008).
- [8] C. Harnett, J. Templeton, K. Dunphy-Gazman, Y. Senousy, and M. Kanouff, *Lab Chip* **8**, 565 (2008).
- [9] H. Zhao and H. H. Bau, *Phys. Rev. E* **75**, 066217 (2007).
- [10] H. Sugioka, *Phys. Rev. E* **81**, 036306 (2010).
- [11] H. Sugioka, *Phys. Rev. E* **81**, 036301 (2010).
- [12] M. C. Fair and J. L. Anderson, *J. Colloid Interf. Sci.* **127**, 388 (1989).
- [13] T. M. Squires and M. Z. Bazant, *J. Fluid Mech.* **509**, 217 (2004).
- [14] A. J. Pascall and T. M. Squires, *Phys. Rev. Lett.* **104**, 088301 (2010).
- [15] M. S. Kilic, M. Z. Bazant, and A. Ajdari, *Phys. Rev. E* **75**, 021502 (2007).
- [16] M. S. Kilic, M. Z. Bazant, and A. Ajdari, *Phys. Rev. E* **75**, 021503 (2007).
- [17] M. Z. Bazant, K. Thornton, and A. Ajdari, *Phys. Rev. E* **70**, 021506 (2004).
- [18] V. Dolejsi, M. Feistauer, and C. Schwab, *Math. Comput. Simul.* **61**, 333 (2003).
- [19] G. Yagawa, Y. Nakabayashi, and H. Okuda, *Parallel Comput.* **23**, 1365 (1997).
- [20] H. Sugioka, *Phys. Rev. E* **86**, 016318 (2012).
- [21] H. Oshima, *J. Colloid Interf. Sci.* **247**, 18 (2002).

- [22] J. A. Levitan, S. Devasenathipathy, V. Studer, Y. Ben, T. Thorsen, T. M. Squires, and M. Z. Bazant, *Colloids Surf. A* **267**, 122 (2005).
- [23] N. G. Green, A. Ramos, A. Gonzalez, H. Morgan, and A. Castellanos, *Phys. Rev. E* **66**, 026305 (2002).
- [24] T. M. Squires, *Lab Chip* **9**, 2477 (2009).
- [25] N. G. Green, A. Ramos, A. Gonzalez, H. Morgan, and A. Castellanos, *Phys. Rev. E* **61**, 4011 (2000).
- [26] S. M. Davidson, M. B. Anderson, and A. Mani, *Phys. Rev. Lett.* **112**, 128302 (2014).
- [27] E. Kartalov and S. Quake, *Nucleic Acids Res.* **32**, 2873 (2004).
- [28] K. Aoki, C. Li, T. Nishiumi, and J. Chen, *J. Electroanal. Chem.* **695**, 24 (2013).
- [29] P. M. Biesheuvel, Y. Fu, and M. Z. Bazant, *Phys. Rev. E* **83**, 061507 (2011).
- [30] P. M. Biesheuvel, M. van Soestbergen, and M. Z. Bazant, *Electrochim. Acta* **54**, 4857 (2009).
- [31] M. van Soestbergen, P. M. Biesheuvel, and M. Z. Bazant, *Phys. Rev. E* **81**, 021503 (2010).
- [32] M. van Soestbergen, *Electrochim. Acta* **55**, 1848 (2010).